ORIGINAL ARTICLE

Lymphatic-Dependent Modulation of the Sensitization and Elicitation Phases of Contact Hypersensitivity

JID Open

Petra Aradi[1], Gábor Kovács[1], Éva Kemecsei[1], Kornél Molnár[1], Stella Márta Sági[1], Zalán Horváth[1], Babak J. Mehrara[2], Raghu P. Kataru[2] and Zoltán Jakus[1]

Allergic contact dermatitis is a common inflammatory skin disease comprising 2 phases. During sensitization, immune cells are activated by exposure to various allergens, whereas repeated antigen exposure induces local inflammation during elicitation. In this study, we utilized mouse models lacking lymphatics in different skin regions to characterize the role of lymphatics separately in the 2 phases, using contact hypersensitivity as a model of human allergic inflammatory skin diseases. Lymphatic-deficient mice exhibited no major difference to single antigen exposure compared to controls. However, mice lacking lymphatics in both phases displayed reduced inflammation after repeated antigen exposure. Similarly, diminished immune response was observed in mice lacking lymphatics only in sensitization, whereas the absence of lymphatics only in the elicitation phase resulted in a more pronounced inflammatory immune response. This exaggerated inflammation is driven by neutrophils impacting regulatory T cell number. Collectively, our results demonstrate that skin lymphatics play an important but distinct role in the 2 phases of contact hypersensitivity. During sensitization, lymphatics contribute to the development of the antigen-specific immunization, whereas in elicitation, they moderate the inflammatory response and leukocyte infiltration in a neutrophil-dependent manner. These findings underscore the need for novel therapeutic strategies targeting the lymphatics in the context of allergic skin diseases.

Keywords: Contact hypersensitivity, Inflammation, Mouse models, Neutrophil granulocytes, Skin lymphatics

Journal of Investigative Dermatology (2024) **144,** 2240–2254; doi:10.1016/j.jid.2024.03.021

INTRODUCTION

The skin functions as a protective barrier organ, shielding the body from external factors, such as pathogens, physical, or chemical agents (Kabashima et al, 2019). Allergic contact dermatitis represents a common inflammatory skin disease characterized by a type IV delayed-type hypersensitivity reaction initiated through repeated exposure to contact allergens (Kaplan et al, 2012; Scheinman et al, 2021). This T cell–mediated immune response manifests as red, dry, itchy skin with papules and vesicles (Kaplan et al, 2012; Martin, 2015; Martin et al, 2011; Novak-Bilić et al, 2018; Scheinman et al, 2021; Vocanson et al, 2009). Contact hypersensitivity (CHS) serves as a well-characterized mouse model for human allergic inflammatory skin diseases, induced by repeated exposure of reactive chemicals containing specific haptens such as oxazolone, 2,4-dinitro-1-fluorobenzene (DNFB), or 2-chloro-1,3,5-trinitrobenzene (TNCB) (Honda et al, 2013; Kaplan et al, 2012; Manresa, 2021). Similarly to the human diseases, the pathogenesis of CHS is divided into 2 phases. First, in the sensitization phase, epidermal Langerhans cells or dermal dendritic cells initiate the immune response in the local lymph nodes by presenting the antigen to naive T cells. Subsequently, during the elicitation phase, re-exposure to the same antigen triggers a cascade of events resulting in the infiltration of effector immune cells, including neutrophils and monocytes, to the site of antigen challenge. This process triggers an inflammatory reaction and tissue damage (Azeem et al, 2020; Honda et al, 2019, 2013). Neutrophils play a crucial role not only in inducing tissue damage during the elicitation phase but are also involved in initiating the sensitization phase of the disease (Strzepa et al, 2020; Weber et al, 2015).

Lymphatics have several well-established roles in regulating immune functions in various contexts, including infectious diseases and lymphedema (Kataru et al, 2019; Oliver et al, 2020; Tammela and Alitalo, 2010). These structures are also involved in maintaining skin homeostasis upon inflammatory challenges (Huggenberger and Detmar, 2011). Although lymphatics have been implicated in dendritic cell trafficking to local lymph nodes, their specific function in initiating the sensitization phase of CHS model has not been thoroughly investigated (Collado-Diaz et al, 2022; Worbs et al, 2017). Previous studies indicated that stimulating lymphangiogenic VEGF-C signaling pathway resulted in reduced inflammatory responses. In these experiments, the administration of recombinant VEGF-C in the keratin 14

[1]*Department of Physiology, Semmelweis University School of Medicine, Budapest, Hungary; and* [2]*Division of Plastic and Reconstructive Surgery, Department of Surgery, Memorial Sloan Kettering Cancer Center, New York, New York, USA*

Correspondence: Zoltán Jakus, Department of Physiology, Semmelweis University School of Medicine, Tűzoltó utca 37-47, Budapest 1094, Hungary. E-mail: jakus.zoltan@semmelweis.hu

Abbreviations: CHS, contact hypersensitivity; DNFB, 2,4-dinitro-1-fluorobenzene; DT, diphtheria toxin; TNCB, 2-chloro-1,3,5-trinitrobenzene

Received 27 July 2023; revised 17 February 2024; accepted 1 March 2024; accepted manuscript published online 27 March 2024; corrected proof published online 16 May 2024

VEGF-A–transgenic mouse model or inducing adenovirus mediated expression of VEGF-C led to the inhibition of chronic skin inflammation (Hagura et al, 2014; Huggenberger et al, 2010). In addition, keratin 14 VEGF-C–overexpressing transgenic mice have significantly reduced acute skin inflammation after allergen-induced delayed-type hypersensitivity reactions (Huggenberger et al, 2011; Schwager and Detmar, 2019). Moreover, some studies using soluble VEGFR3 (the receptor of VEGF-C)-blocking antibodies demonstrated an increased inflammatory response in chronic cutaneous inflammation (Hagura et al, 2014; Huggenberger et al., 2010). These findings suggest the complex and context-dependent roles of lymphatics in modulating inflammatory processes.

The studies mentioned earlier also indicated a crucial role for the VEGF-C–VEGFR3 signaling axis in reducing local skin inflammation in CHS by promoting lymphatic growth. However, limitations in previous methodologies, such as uncontrollable expression of VEGF-C or VEGFR3 ligands and potential nonspecific effects of blocking antibodies, prompted the need for a more specific investigation. In addition, these experimental models have not been studied in a comparable way to characterize the role of lymphatics separately in the 2 phases of CHS and mostly focused on the acute effect of VEGF-C–VEGFR3 axis stimulation or inhibition in the pathogenesis of skin diseases.

In this study, our primary objective was to characterize the importance of local lymphatic structures in TNCB-induced CHS development. First, we rigorously tested the possible involvement of local skin lymphatics in the CHS pathogenesis using a genetic mouse model with a complete absence of lymphatics throughout the skin. Then, to dissect the role of the lymphatics separately in the sensitization and elicitation phases, we employed a strategy to delete lymphatics with spatial and temporal specificity. Our results indicate the diverse and critical roles of lymphatics in the 2 phases of CHS. Specifically, lymphatics contribute to the development of antigen-induced immunization during the sensitization phase, whereas in the elicitation phase, they regulate the inflammatory response and immune cell infiltration, dependent on neutrophils. These findings highlight the necessity for refined therapeutic approaches targeting lymphatics in the context of allergic skin diseases.

RESULTS

Characterization of the genetic mouse models used for studying the role of lymphatics in the 2 distinct phases of CHS

We employed multiple mouse strains to investigate the role of lymphatics in the 2 distinct phases of CHS. The *Vegfr3*$^{kd/+}$ mouse is carrying a kinase-dead allele of the *Flt4* gene encoding VEGFR3, which is a key factor in the development and maintenance of lymphatic vessels and is primarily expressed by lymphatic endothelial cells in adults (Kaipainen et al, 1995; Karkkainen et al, 2001; Rauniyar et al, 2018). This mutation causes abnormal lymphangiogenesis, resulting in the absence of skin lymphatics in these mice (Christ and Jakus, 2023; Karkkainen et al, 2001). To confirm the suitability of the *Vegfr3*$^{kd/+}$ mouse strain as a model for lymphatic deficiency, we conducted a detailed histological analysis. Crossbreeding *Vegfr3*$^{kd/+}$ mice with the *Prox1*^{GFP} lymphatic reporter mouse strain facilitated the visualization of lymphatic structures (Choi et al, 2011). We observed the lack of lymphatics in the ear (Figure 1a and Supplementary Figure S1b–d) and back skin but not in other tissues, including the lungs and the small intestine (Supplementary Figure S1a and c). Importantly, the blood vessels in all the tissues of *Vegfr3*$^{kd/+}$ mice remained unaffected (Supplementary Figure S1c and d). In addition, increased immune cell infiltration was not observed in the ears of *Vegfr3*$^{kd/+}$ mice compared with that in the wild-type controls (Figure 1b and Supplementary Figure S1e and f). These findings indicate that the *Vegfr3*$^{kd/+}$ mouse strain can serve as a reliable model to study the role of lymphatics in both phases of CHS. In subsequent sections, we will refer to *Vegfr3*$^{kd/+}$ mice as lymphatic-deficient in both phases.

Next, we compared the inflammation after single and repeated antigen treatments to induce CHS in the previously introduced mouse model with intact lymphatics on a NMRI genetic background. The results revealed a substantial increase in ear thickness after repeated antigen treatment compared with that observed after a single antigen exposure (Figure 1c). Histological examination using H&E staining demonstrated significant cell infiltration into the ear tissue after repeated antigen exposure (Figure 1d). Further characterization through flow cytometry confirmed a marked increase in leukocyte infiltration, particularly neutrophils and T cells (Figure 1e).

To dissect the role of lymphatics separately in the 2 phases of CHS, we also performed an alternative strategy to selectively eliminate lymphatic vessels with spatial–temporal specificity. To this end, we used Flt4-CreER^{T2}; *iDTR*$^{fl/+}$ mice (crossed with the *Prox1*^{GFP} lymphatic reporter strain for the visualization of lymphatics), in which the expression of the diphtheria toxin (DT) receptor in the lymphatic endothelial cells can be induced by tamoxifen administration, and local DT injection triggers the deletion of lymphatics at designated sites (Buch et al, 2005; Choi et al, 2011; Gardenier et al, 2016; Martinez-Corral et al, 2016). First, to characterize the model, we injected DT into the ear of tamoxifen-treated Flt4-CreER^{T2}; *iDTR*$^{fl/+}$ mice. Eight days after injection, the lymphatic vessels were visualized using the *Prox1*^{GFP} signal and anti-LYVE1 immunostaining. The lymphatic vessels were successfully deleted in the ear (Figure 1f and Supplementary Figure S2b–d), with no effect on the contralateral side injected with PBS as a control nor in other organs, including back skin, lungs, and the small intestine (Figure 1f and Supplementary Figure S2a and c). We also demonstrated that DT injection into the mouse ear does not result in local blood vessel deletion or proliferation (Supplementary Figure S2c and d). Moreover, moderated immune cell infiltration, primarily CD3-positive cells, was detected in the ear (Figure 1g and Supplementary Figure S2e). H&E staining showed the development of edema in the ear but not in the other tissues (Supplementary Figure S2f). The data presented before show that the Flt4-CreER^{T2}; *iDTR*$^{fl/+}$ mouse line can be used to delete the lymphatics in specific tissues locally to generate the absence of lymphatics either in the sensitization or the elicitation phase of CHS. We will refer to the DT-injected mice as lymphatic-deficient in sensitization phase or lymphatic-deficient in elicitation phase, respectively.

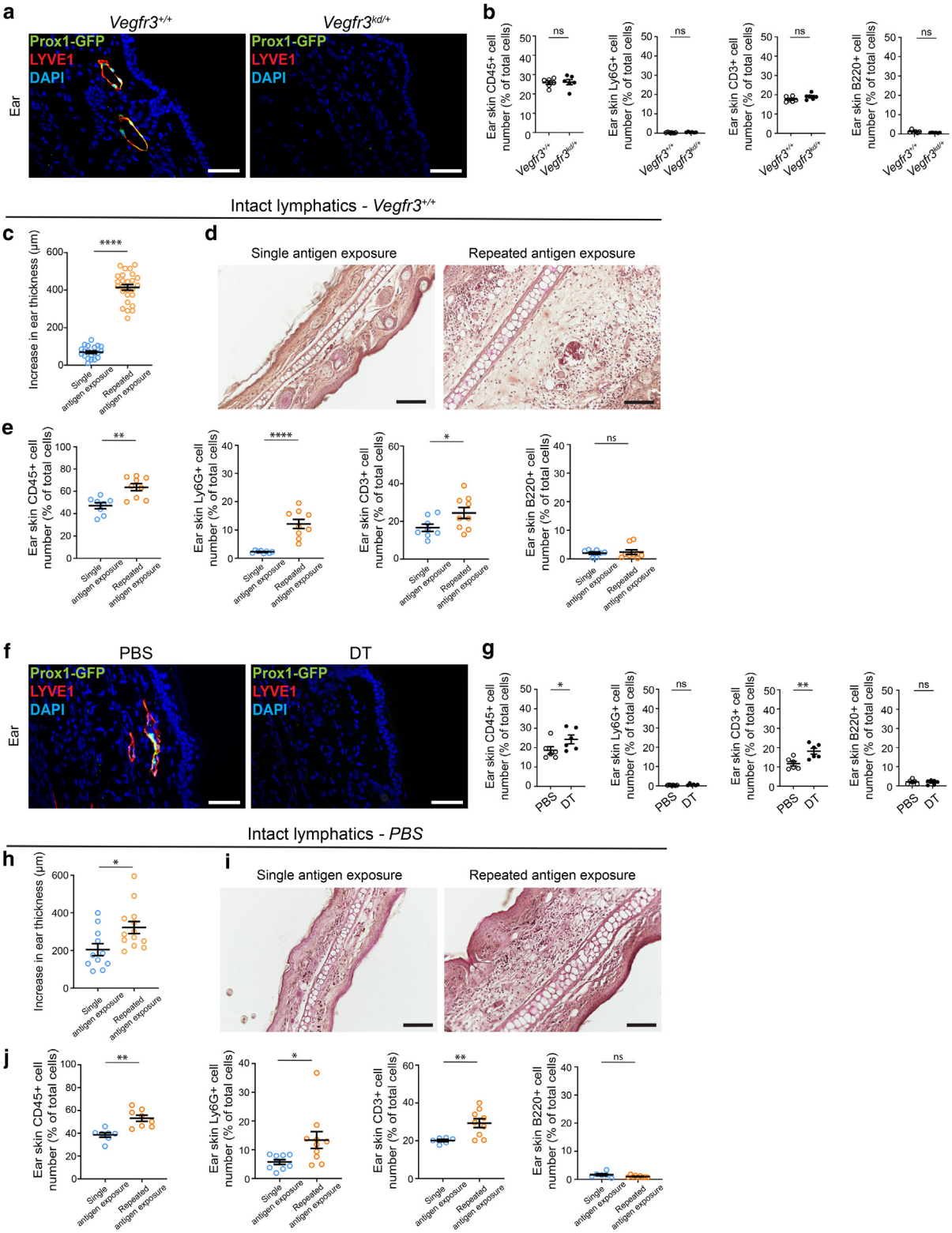

Figure 1. Characterization of contact hypersensitivity in 2 different mouse models. **(a)** Anti-GFP and anti-LYVE1 fluorescent immunostaining of paraffin-based sections of ear of *Prox1*^{GFP} lymphatic reporter *Vegfr3*$^{+/+}$ and *Vegfr3*$^{kd/+}$ mice. Bars = 50 μm; n = 4 for each group. **(b)** Quantitative flow cytometry data for immune cells ($P = .8754$ for CD45$^+$ cells, $P = .0925$ for Ly6G$^+$ cells, $P = .1332$ for CD3$^+$ cells, and $P = .0654$ for B220$^+$ cells; 2-tailed, unpaired *t*-test; mean ± SEM; n = 6 mouse ears for each group). **(c)** The increase in ear thickness of mice with intact lymphatics (*Vegfr3*$^{+/+}$) ($P = 4.4721 \times 10^{-22}$; 2-tailed, unpaired *t*-test; mean ± SEM; n = 20 and n = 26 for the groups after single and repeated antigen exposure, respectively). **(d)** H&E histology of ear sections. Bars = 100 μm; n = 8 and n = 12 for the groups with single and repeated antigen exposure, respectively. **(e)** Quantitative data for immune cells from ear skin by flow cytometry ($P = .0013$ for CD45$^+$ cells, $P = 4.2370 \times 10^{-5}$ for Ly6G$^+$ cells, and $P = .0460$ for CD3$^+$ cells; 2-tailed, unpaired *t*-test; mean ± SEM; $P = .4817$ for B220$^+$ cells; Mann–Whitney *U* test; mean ± SEM; n = 8 and n = 9 for the groups with single and repeated antigen exposure, respectively). **(f)** Anti-GFP and anti-LYVE1 fluorescent immunostaining of *Prox1*^{GFP} lymphatic reporter Flt4-CreER^{T2}; *iDTR*$^{fl/+}$ mouse ear 8 days after the first PBS or DT injection. Bars = 50 μm; n = 3 for

To assess the severity of the inflammation in comparison with that in the other mouse strain, we examined the CHS model on the C57Bl/6 genetic background in ears with intact lymphatics, injected with PBS. The ear thickness exhibited an increase after repeated antigen treatment in contrast to single antigen exposure (Figure 1h). H&E staining verified the elevated infiltration of immune cells (Figure 1i), which phenomenon was further quantified by flow cytometry. Similar to the other mouse strain, there was a significant increase in leukocyte infiltration, particularly in neutrophils and T cells (Figure 1j).

It is important to note that there was no difference in the inflammatory response between the 2 genetic backgrounds (NMRI and C57Bl/6) without any prior injection after repeated antigen exposure, showing that the 2 mouse strains are comparable (Supplementary Figure S3a and b). Furthermore, we studied the antigen specificity, and our results indicated that TNCB-sensitized mice challenged with a different antigen, namely DNFB, did not show a significant difference in ear thickness and immune cell infiltration from the control group (Supplementary Figure S3c and d), indicating the importance of the exposure to the same antigen for the development of CHS, whereas repeated DNFB treatment effectively induced CHS, as described previously in rats (Prop et al, 1986).

These results highlight that in contrast to single antigen exposure, repeated antigen treatments lead to robust inflammation in the CHS model. Moreover, both mouse strains showed specific and dramatic inflammatory phenotypes upon the repeated antigen exposure and responded similarly to antigen treatment. Therefore, these data support that the results of the subsequent experiments are comparable.

Single antigen exposure does not induce a pronounced inflammatory reaction in mouse models with lymphatic deficiency

Next, we investigated whether the absence of lymphatics influences the skin response to the single antigen exposure in our mouse models. The ear thickness of mice with lymphatic deficiency in both phases and only in elicitation phase was significantly increased compared with the ears with intact lymphatics (Supplementary Figures S4a and b and S5a and b). Notably, this increase was not accompanied by a marked immune cell infiltration, as revealed by anti-CD45 and anti-GR1 immunostainings (Supplementary Figures S4c and S5c). Of note, acetone treatment of the ear as a vehicle control (labeled as no exposure) did not affect ear thickness significantly (Supplementary Figures S4a and b and S5a and b). Whole-mount and anti-LYVE1 immunostainings demonstrated the absence of lymphatics after single antigen challenge in mice with lymphatic deficiency in both phases and only in elicitation phase. However, the single antigen exposure did not affect the structure of lymphatic vessels in the control ears with intact lymphatics (Supplementary Figures S4d–f and S5d–f).

In addition, we quantified the immune cells by flow cytometry from digested single-treated ear samples. Apart from an increase in T cell numbers observed only in mice lacking lymphatic vessels in the elicitation phase (consistent with our previous data shown in Figure 1g), no significant changes were detected in the numbers of various immune cell populations (Supplementary Figures S4g and S5g). Then, we measured cytokine levels in the supernatant of the digested ear samples using cytokine array. The results indicated no significant differences in cytokine levels in lymphatic-deficient mice after single antigen exposure compared with those in the controls with intact lymphatics (Supplementary Figures S4h and i and S5h and i).

In conclusion, lymphatic deficiency does not significantly alter immune cell composition or cytokine levels in response to single antigen exposure in mouse models.

Decreased inflammation after repeated antigen treatment in mice lacking lymphatics in both phases of CHS

We utilized the *Vegfr3*$^{kd/+}$ mice lacking lymphatics in skin during both sensitization and elicitation phases of the antigen exposures to investigate the pathogenesis of CHS (Figure 2a). These mice showed a less dramatic increase in ear thickness after repeated antigen exposure compared with mice with intact lymphatics (Figure 2b). The effect of the second antigen exposure in inflammatory responses is calculated by subtracting the mean of the corresponding control group after single antigen exposure from the individual data points after repeated exposure, colored purple in the subsequent sections (Figure 2b). In addition, mice lacking lymphatics had a much less pronounced immune cell infiltration, as shown by H&E staining (Figure 2c) and anti-CD45 and anti-GR1 immunostainings (Figure 2d and e). To characterize the infiltrating immune cell populations more comprehensively, flow cytometry was performed. Mice lacking lymphatics in both phases showed a significant reduction in the infiltration of CD45-positive leukocytes and Ly6G-positive cells representing neutrophils, whereas no significant difference was detected in the number of T cells and B cells (Figure 2f). In mice with intact lymphatics, repeated antigen treatment induced several proinflammatory cytokines (including IFN-γ, IL-1β) and chemokines (including IP-10, JE, MCP-5, MIP1α/β, RANTES), contributing to the recruitment of T cells, dendritic cells, and monocytes. However, the levels of most of these cytokines were significantly lower in mice lacking lymphatics (Figure 2g and h). Even after repeated antigen exposure, lymphatic vessels remained absent in the ear with lymphatic deficiency (Supplementary Figure S6a, b, and d). However,

each group. **(g)** Immune cells quantified by flow cytometry after the digestion of ears 8 days after the first PBS and DT injection ($P = .0254$ for CD45$^+$ cells, $P = .2432$ for Ly6G$^+$ cells, $P = .0073$ for CD3$^+$ cells, and $P = .4028$ for B220$^+$ cells; 2-tailed, paired *t*-test; mean ± SEM; n = 6 mouse ear for each group). **(h)** The increase in ear thickness of mice with intact lymphatics (PBS injected, Flt4-CreER^{T2}; *iDTR*$^{fl/+}$) ($P = .0174$; 2-tailed, unpaired *t*-test; mean ± SEM; n = 11 and n = 13 for the groups after single and repeated antigen exposure, respectively). **(i)** H&E staining of ear sections with intact lymphatics. Bars = 100 μm; n = 11 and n = 13 for the groups with single and repeated antigen exposure, respectively. **(j)** Quantitative data for immune cell numbers ($P = .0011$ for CD45$^+$ cells, $P = .0088$ for CD3$^+$ cells, and $P = .0950$ for B220$^+$ cells; 2-tailed, unpaired *t*-test; mean ± SEM; n = 6 and n = 9 for the groups with single and repeated antigen exposure, respectively; $P = .0101$ for Ly6G$^+$ cells; Mann–Whitney *U* test; mean ± SEM; n = 9 and n = 10 for the groups with single and repeated antigen exposure, respectively). DT, diphtheria toxin; ns, not significant.

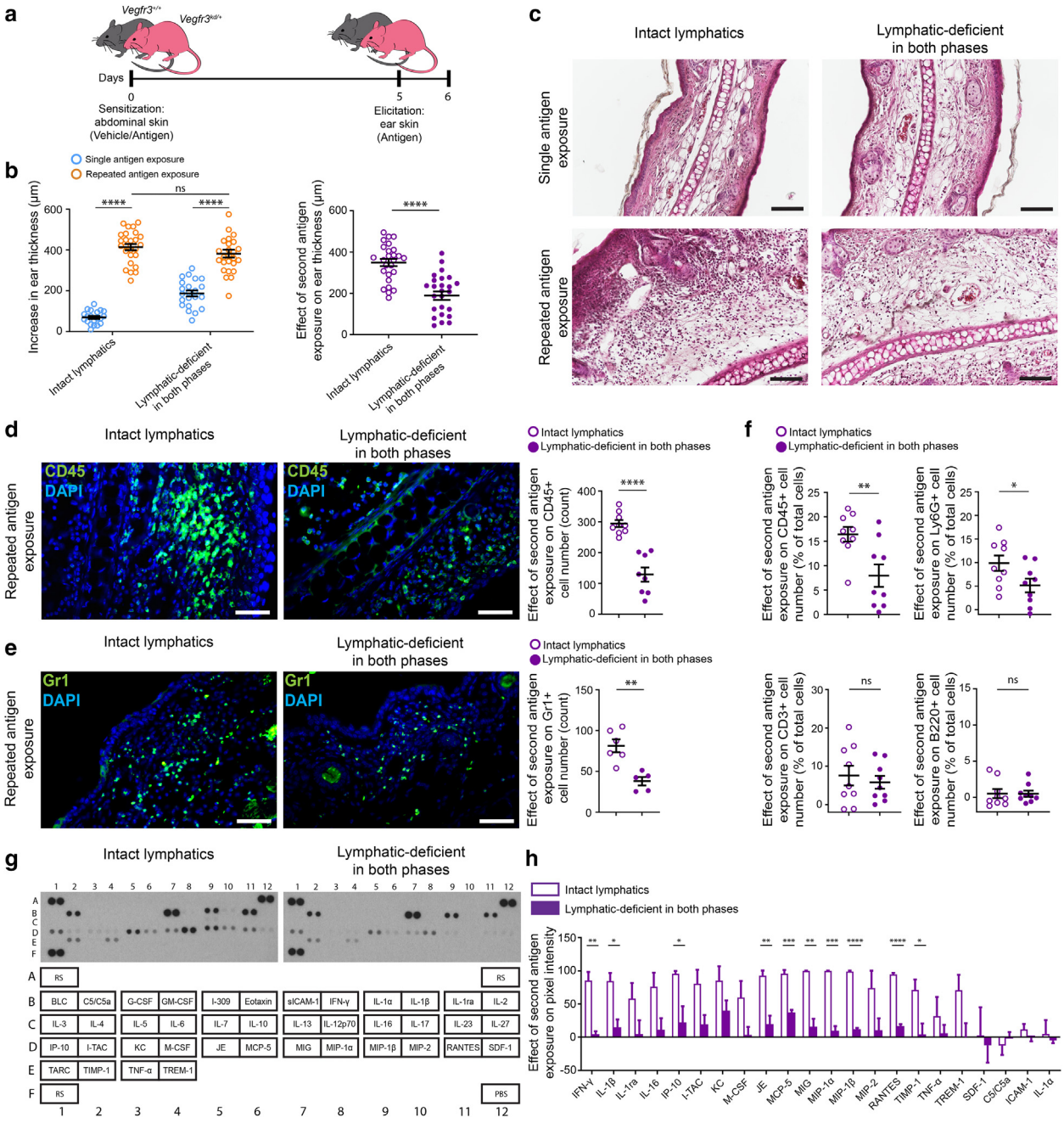

Figure 2. Effect of repeated antigen exposure in mice lacking lymphatic vessels both in the sensitization phase and in the elicitation phase. **(a)** Mice with normal lymphatics or dermal lymphatic deficiency (marked with pink color) were treated with antigen on the abdominal skin, and 5 days after exposure, antigen treatment was repeated on the ear skin. **(b)** The increase in ear thickness of mice with intact lymphatics and lymphatic deficiency in both phases (2-way ANOVA with Tukey's multiple comparisons test; mean ± SEM; n = 20 and n = 26 for the groups after single and repeated antigen exposure, respectively; normal vs lymphatic deficiency after single exposure: $P < .0001$; normal lymphatics after single vs repeated exposure: $P < .0001$; normal vs lymphatic deficiency after repeated exposure: $P = .4050$; lymphatic deficiency after single vs repeated exposure: $P < .0001$). The effect of the repeated antigen exposure on ear thickness is calculated by subtracting the mean of the corresponding control group values after single exposure ($P = 2.9813 \times 10^{-7}$ 2-tailed, unpaired *t*-test; mean ± SEM; n = 26 for each group). **(c)** H&E histology of ear skin sections. Bars = 100 μm; n = 12 for each group. **(d)** CD45-expressing immune cells in ear sections visualized by fluorescence microscopy. Bars = 50 μm; $CD45^+$ cell numbers ($P = 7.8594 \times 10^{-6}$; 2-tailed, unpaired *t*-test; mean ± SEM; n = 9 and n = 8 for the groups with intact and lymphatic deficiency in both phases, respectively). **(e)** Same as **d** for GR1-expressing cells ($P = .0018$; 2-tailed, unpaired *t*-test; mean ± SEM; n = 6 and n = 5 for the groups with intact lymphatics and lymphatic-deficient group in both phases, respectively). **(f)** Quantitative flow cytometry data for immune cell numbers from ears ($P = .0071$ for $CD45^+$ cells, $P = .0467$ for $Ly6G^+$ cells, and $P = .5720$ for $CD3^+$ cells; 2-tailed, unpaired *t*-test; mean ± SEM; n = 9 for each group; $P = .6048$ for $B220^+$ cells; Mann–Whitney *U* test; mean ± SEM; n = 9 for each group). **(g)** Cytokine array to detect cytokine expression in ear tissue supernatants. The representative images show the arrangement of the cytokines in duplicates (n = 3). Data are shown from a 5-minute exposure to the X-ray film containing our experimental groups. **(h)** Summary graph of the quantification of the cytokine array demonstrating the effect of the second antigen exposure over the first (2-tailed, unpaired *t*-test; mean ± SEM; n = 3 for each group). ns, not significant; RS, reference spot.

the lymphatic structure in the control ear exhibited significant alterations compared with ears treated with a single application, showing an increased number and dilation under inflammatory conditions (Supplementary Figure S6a–c).

Therefore, our results indicate that the lack of lymphatics during both phases of CHS leads to a reduced immune response after repeated antigen exposure.

Lacking lymphatics only in the sensitization phase of CHS leads to reduced inflammation after repeated antigen treatment

Although previous data suggest that the lymphatic system is an important contributor to inflammation during CHS (Hagura et al, 2014; Huggenberger et al, 2011, 2010; Schwager and Detmar, 2019), it remains elusive whether the presence of lymphatics is equally important during the 2 phases of CHS. To study the role of lymphatics in the sensitization phase of CHS, local deletion of lymphatics was induced in the hind paw of Flt4-CreER^{T2}; *iDTR$^{fl/fl}$* mice with DT treatment. To achieve this, we ablated the lymphatics in the hind limbs during the sensitization phase, and elicitation was performed in the ear skin (Figure 3a). The deletion of lymphatics was confirmed by anti-LYVE1 and anti-PDPN immunostainings (Supplementary Figure S7a), inducing edema formation in hind limb (Supplementary Figure S7b). Mice lacking lymphatics exhibited a less pronounced increase in ear thickness and cell infiltration after repeated antigen exposure in the ears than the control mice (Figure 3b and c), consistent with findings from our previous mouse model. Importantly, these mice had lower CD45$^+$ and GR1$^+$ immune cell infiltration (Figure 3d and e). Flow cytometry confirmed the reduced infiltration of CD45$^+$ and Ly6G$^+$ cells in mice with lymphatic deficiency compared with that in mice with intact lymphatics, whereas CD3$^+$ and B220$^+$ cell populations showed no significant difference between these groups (Figure 3f).

Moving forward, we sought to characterize the regional lymph node of the hind limbs where the sensitization phase was induced. The size of the inguinal lymph nodes on the treated side of lymphatic-deficient mice was significantly smaller after the repeated antigen exposure compared with that in the mice with intact lymphatics (Figure 3g), indicating a diminished immune response. However, this effect was not detectable on the other untreated side of the same mouse, showing a local effect of the antigen treatment. No major alterations in the structure of lymphatic and blood vessels could be detected upon staining histological slides with anti-LYVE1 and anti-CD31 antibodies of the inguinal lymph node (Figure 3g), showing that despite the DT injection, the lymphatics and blood vessel structures within the lymph node remained intact.

Collectively, the data presented earlier suggest that skin lymphatics contribute to the immunization against the antigens in the sensitization phase during the development of CHS.

Lack of lymphatics in the sensitization phase attenuates naive T cell activation

Antigen-presenting cells play an important role in the sensitization phase of CHS by presenting the contact antigen to naive T cells in the lymph nodes, which is associated with elevated IFN-γ secretion (Kabashima et al, 2019; Kaplan et al, 2012). Therefore, we investigated whether lymphatic deficiency in the sensitization phase would affect the activation of the naive T cell population in the regional lymph node by monitoring the IFN-γ production of these cells ex vivo. After the first antigen exposure to the hind limb with intact lymphatics or lymphatic deficiency, lymph nodes were isolated, and cell suspension was produced. The second exposure to the water-soluble antigen was performed on the cell suspension in an in vitro restimulation assay (passive CHS model). Cells from mice with intact lymphatics showed significantly higher IFN-γ production followed by subtracting the control group than cells from mice lacking lymphatics in the sensitization phase in the passive CHS model (Figure 4a).

Therefore, our findings indicate that besides regulating the immunization in the sensitization phase after repeated antigen exposures, the lymphatics also contribute to the T cell activation in the inguinal lymph nodes.

Lacking lymphatics only in the elicitation phase of CHS leads to augmented inflammation after repeated antigen treatments

Next, we aimed to determine the role of lymphatics specifically in the elicitation phase. In a repeated antigen exposure regimen, sensitization was induced by treating the abdomen with intact lymphatics, followed by induction of the elicitation in the ear with intact lymphatics or with local lymphatic deficiency induced by DT injection (Figure 5a). Surprisingly, mice lacking lymphatics in the elicitation phase showed increased swelling of the ear compared with that of contralateral ears with intact lymphatics (Figure 5b), accompanied by a higher number of infiltrating cells (Figure 5c). We extended our observation period to 4 days after the challenge to monitor the inflammation, revealing a constant increase in ear thickness in both the groups with intact lymphatics and lymphatic deficiency. However, the severity of inflammation was notably elevated on each day in mice with lymphatic deficiency (Figure 5d). Immunostaining of ear sections also confirmed that mice lacking lymphatics in the elicitation phase had increased CD45$^+$ and GR1$^+$ immune cell infiltration (Figure 5e and f). In addition, flow cytometry analysis of digested ear samples showed a significantly increased CD45$^+$ and Ly6G$^+$ cell count in mice in which lymphatics were deleted only in the elicitation phase, a significant difference that persisted up to 4 days after elicitation (day 9). Moreover, no significant difference was observed in CD3$^+$ and B220$^+$ cell populations after repeated antigen exposure (Figure 5g). The increased inflammation in mice with no lymphatics was also confirmed by a cytokine array (Figure 5h and i) for ear tissue supernatants showing massively increased chemokine (MCP-5, MIG, MIP-1α/β, MIP-2, RANTES) and proinflammatory cytokine (IFN-γ, IL-1β) production. Notably, after repeated antigen exposure, the lymphatics did not re-emerge in lymphatic-deficient mice despite the increased inflammation (Supplementary Figure S8a–d).

We further investigated antigen specificity in the CHS mouse model by examining mice lacking lymphatics. Augmented ear swelling was observed upon treatment with the same antigen compared with when different haptens were applied (Supplementary Figure S3c). Immune cell

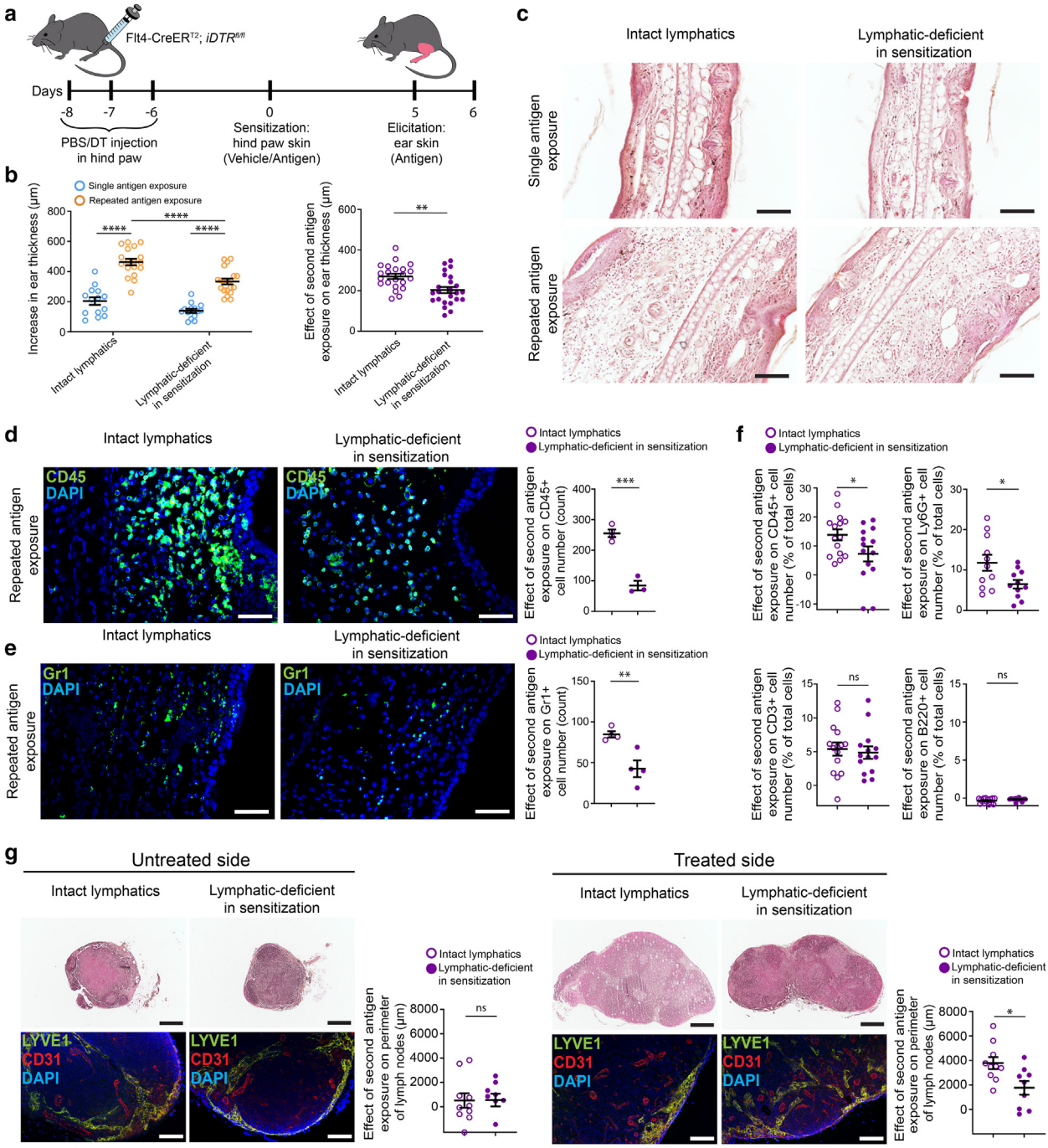

Figure 3. Effect of repeated antigen exposure in mice lacking lymphatic vessels in the sensitization phase. **(a)** Flt4-CreER^{T2}; *iDTR*$^{fl/fl}$ mice were injected with DT into the hind paw skin for 3 days. As a control, PBS was administered to a littermate. Mice with normal lymphatics or local lymphatic deficiency in the hind paw (marked with pink color) were treated with vehicle or antigen on the hind paw skin, and 5 days after exposure, antigen treatment was repeated on ear skin. **(b)** The increase in ear thickness (2-way ANOVA with Tukey's multiple comparisons test; mean ± SEM; n = 14 and n = 18 for the groups after single and repeated exposure; normal lymphatics vs lymphatic deficiency after single exposure: $P = .1755$; normal lymphatics after single vs repeated exposure: $P < .0001$; normal lymphatics vs lymphatic deficiency after repeated exposure: $P < .0001$; lymphatic deficiency after single vs repeated exposure: $P < .0001$). The effect of the second antigen exposure on ear thickness ($P = .0015$; 2-tailed, unpaired *t*-test; mean ± SEM; n = 18 and n = 20 for the groups with intact lymphatics and lymphatic deficiency only in sensitization). **(c)** H&E histology of ear skin sections. Bars = 100 μm; n = 8 for each group. **(d)** CD45-expressing cells in ear sections. Bars = 50 μm; n = 4 for each group. Number of CD45$^+$ cells in ear quantified on the basis of fluorescent immunohistology ($P = .0003$; 2-tailed, unpaired *t*-test; mean ± SEM; n = 4 for each group). **(e)** Same as **d** for GR1-expressing cells. Bars = 50 μm; n = 4 for each group. Number of GR1$^+$ cells in ear ($P = .0084$; 2-tailed, unpaired *t*-test; mean ± SEM; n = 4 for each group). **(f)** The effect of the second antigen exposure to the CD45$^+$, Ly6G$^+$, CD3$^+$, and B220$^+$ immune cells ($P = .0489$ for CD45$^+$ cells; $P = .0279$ for Ly6G$^+$ cells, and $P = .6934$ for CD3$^+$ cells; 2-tailed, unpaired *t*-test; mean ± SEM; $P = .2012$ for B220$^+$ cells; Mann–Whitney *U* test; mean ± SEM; n = 11 for the group with intact lymphatics and n = 15 for the group with lymphatic deficiency only in elicitation). **(g)** Mice with normal lymphatics or local lymphatic deficiency in the hind paw were treated with antigen on the hind paw, and 5 days after exposure, antigen treatment was repeated on ear skin. H&E histology of inguinal lymph nodes from the untreated and the treated side of mice with intact lymphatics or lymphatic deficiency. Bars = 500 μm; n = 8 for each group. Shown is the anti-LYVE1 and anti-CD31 fluorescent immunostaining of the inguinal lymph nodes

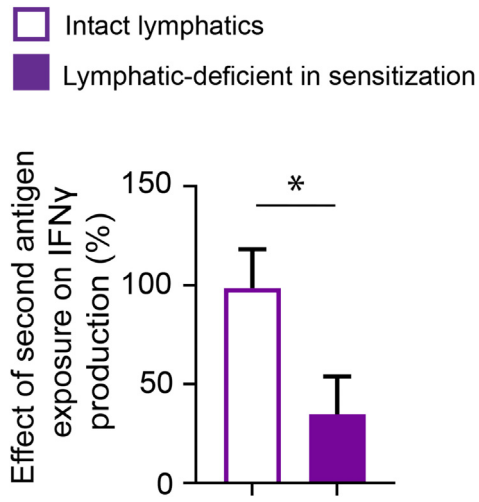

Figure 4. IFN-γ production of the regional lymph node cells of mice lacking lymphatic vessels in the sensitization phase after repeated antigen treatment. Mice with normal lymphatics or local lymphatic deficiency in the hind paw were treated with vehicle or antigen on the hind paw, and 5 days after exposure, inguinal lymph nodes were collected and prepared into cell cultures. Then, the cell cultures were treated with vehicle or with water-soluble antigen (TNBS), and IFN-γ values in the supernatant were measured by ELISA. Normalized concentration of IFN-γ in supernatants after the repeated antigen treatment is shown in cell cultures containing T cells, collected from lymph nodes of mice with intact lymphatics or lymphatic deficiency in sensitization. The graph demonstrates the effect of the second antigen exposure to the IFN-γ levels calculated by subtracting the mean of corresponding control groups after in vivo antigen exposure ($P = .0205$; Mann–Whitney *U* test; mean ± SEM; n = 7 and n = 8 for the groups with intact lymphatics and lymphatic deficiency, respectively).

infiltration was also pronounced in the ears of lymphatic-deficient mice in elicitation with repeated DNFB treatment compared with that in the ears with intact lymphatics, similar to repeated TNCB treatment, whereas repeated DNFB did not significantly alter lymphatic-dependent changes in ear thickness (Supplementary Figure S3c and d).

Taken together, our results suggest that skin lymphatics play an anti-inflammatory role during the development of the elicitation phase of CHS.

Neutrophil granulocytes contribute to the exaggerated inflammation in lymphatic deficiency during elicitation phase

An exaggerated inflammation was observed in mouse ears lacking lymphatics during the elicitation phase. In the subsequent experiment, we explored the role of neutrophil granulocytes in this heightened inflammatory response. To answer this question, neutrophil granulocytes were depleted using an anti-Ly6G antibody just before the elicitation phase, with an isotype antibody serving as a control treatment. The CHS model was then induced as previously described (Figure 6a). To confirm the success of neutrophil depletion, we measured immune cell count in peripheral blood before and after the antibody administration at 3 different time points. Neutrophil numbers were indeed reduced, approaching zero, whereas other immune cells such as B cells remained unaffected (Figure 6b), suggesting the success of neutrophil depletion in our model system.

A reduced tendency for inflammatory response was noted in the absence of neutrophils after single antigen exposure, although this did not lead to a significant reduction in ear thickness or $CD45^+$ and $CD25^+$ immune cell infiltration, despite the clear depletion of neutrophils (Figure 6c and d).

After the induction of inflammatory skin disease with repeated antigen exposure, the increase in ear thickness was significantly attenuated in ears with lymphatic deficiency due to the absence of neutrophils, reaching levels comparable with those in ears with intact lymphatics (Figure 6e). This observation was supported by the flow cytometry measurement that compared with the lymphatic-deficient isotype, control-treated group showed decreased $CD45^+$ immune cell infiltration in the lymphatic-deficient and Ly6G-depleted group, whereas the neutrophils were clearly depleted (Figure 6f). Furthermore, the number of $CD25^+$ regulatory T cells notably increased after the repeated antigen exposure, which was significantly enhanced in ears with lymphatic deficiency. Remarkably, the regulatory T cell number was strongly diminished after neutrophil depletion in the absence of lymphatic vessels, suggesting that their recruitment was influenced by neutrophils (Figure 6f).

On the basis of these findings, we can conclude that neutrophils play a significant role in the development of exaggerated inflammation in the case of lymphatic deficiency during elicitation phase. Moreover, these cells also have an impact on the regulatory T cells during inflammatory conditions.

DISCUSSION

In this study, we characterized the immunomodulatory effects of local lymphatics in the sensitization and elicitation phases of TNCB-induced CHS. For this purpose, we used genetic mouse models with the absence and inducible elimination of local skin lymphatics. The *Vegfr3*$^{kd/+}$ model showed a complete lack of lymphatics in the skin, demonstrated in the ear and back skin (Figure 1a and b and Supplementary Figure S1a–d) and as described before (Christ and Jakus, 2023; Karkkainen et al, 2001). Although paraffin-based histology did not reveal alterations in the lymphatic structures of internal organs, including the lungs and the small intestine (Supplementary Figure S1), a more detailed visualization of the lymphatic morphology was needed in our recent study to characterize the changes in these internal organs (Christ and Jakus, 2023). In the Flt4-CreER^{T2}; *iDTR*$^{fl/fl}$ model, local administration of DT efficiently eliminated skin lymphatics in a site-dependent manner compared with that in the PBS-treated control mice (Figure 1 and Supplementary Figure S2), consistent with previous findings (Gardenier et al, 2016; Szőke et al, 2021), whereas the other organs were not affected.

As described before (Gardenier et al, 2016), we detected a significant but moderate increase in the infiltration of $CD45^+$

demonstrating the structure of blood and lymphatic vessels. Bars = 100 μm; n = 8 for each group. The effect of repeated antigen exposure to the perimeter of the inguinal lymph node ($P = .9612$ for inguinal lymph nodes on untreated side, $P = .0136$ for inguinal lymph nodes on the treated side; 2-tailed, unpaired *t*-test; mean ± SEM; n = 10 and n = 9 for the groups with intact lymphatics and lymphatic-deficient, respectively). DT, diphtheria toxin; ns, not significant.

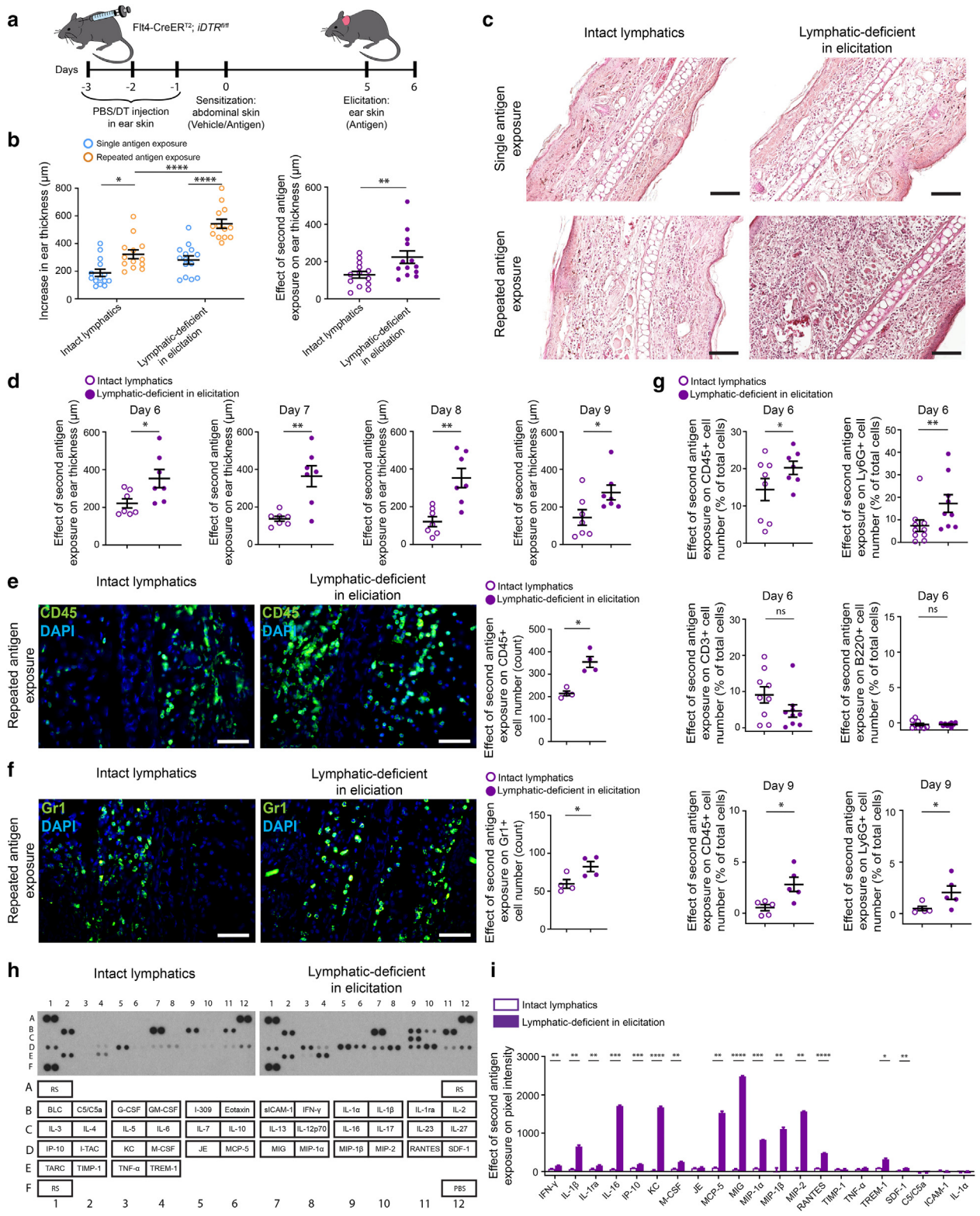

Figure 5. Effect of repeated antigen exposure in mice lacking lymphatics in the elicitation phase. **(a)** Flt4-CreER^{T2}; *iDTR$^{fl/fl}$* mice were injected with DT into ear skin for 3 days. As a control, PBS was administered into the contralateral ear of the same mouse. Mice with normal lymphatics or local lymphatic deficiency in ear skin (marked with pink color) were treated with antigen on the abdominal skin, and 5 days after exposure, antigen treatment was repeated on ear skin. **(b)** The increase in ear thickness after antigen exposure (2-way ANOVA with Tukey's multiple comparisons test; mean ± SEM; n = 14 and n = 13 for the groups after single and repeated exposure, respectively; normal lymphatics vs lymphatic deficiency after single exposure: $P = .1339$; normal lymphatics after single vs repeated exposure: $P = .0150$; normal lymphatics vs lymphatic deficiency after repeated exposure: $P < .0001$; lymphatic deficiency after single vs repeated exposure: $P < .0001$).The effect of the repeated antigen exposure on ear thickness ($P = .0024$; Wilcoxon signed-rank test; mean ± SEM; n = 13 for each group). **(c)** H&E histology of ear sections. Bars = 100 μm; n = 13 for each group. **(d)** The effect of the repeated antigen exposure on ear thickness at different time points ($P = .0469$ for day 6, Wilcoxon signed-rank test; $P = .0053$ for day 7, 2-tailed paired *t*-test; $P = .0026$ for day 8, 2-tailed paired *t*-test; $P = .0313$ for day 9,

immune cells and $CD3^+$ T cells at the site of the DT injection, even in the absence of additional antigen treatments (Figure 1f and g). Notably, despite CHS being a T cell–mediated inflammatory skin disease, this modestly increased T cell number did not escalate further with repeated antigen exposure compared with that in ears with intact lymphatics (Figure 5g). This rise in the infiltration of T cells was not detectable in the skin of *Vegfr3*$^{kd/+}$ mice lacking lymphatics in the entire skin compared with that in the *Vegfr3*$^{+/+}$ mice (Figure 1b and Supplementary Figure S1e). It should be noted that single and repeated antigen exposures did not induce the regrowth of lymphatics in our animal models with lack of lymphatics (Supplementary Figures S4d–f; S5d–f; S6a, b, and d; and S8a, b, and d). In parallel, inflammation-dependent morphological changes of skin lymphatics were detectable in mice with intact lymphatics after repeated antigen treatment, including dilation and increased number of lymphatic vessels (Supplementary Figures S6a–c and S8a–c). The 2 mouse strains utilized are ideal models for testing the role of the lymphatic vessels separately in the 2 phases of CHS. We confirmed that our CHS protocol, involving repeated antigen exposure, induces ear thickening and immune cell infiltration in mice in the same way either on the NMRI (*Vegfr3*$^{+/+}$) or on the C57Bl/6 (Flt4-CreER^{T2}; *iDTR*$^{fl/fl}$ treated with PBS) genetic background (Figure 1c–e and h–j and Supplementary Figure S3), indicating that the applied disease model is robust, stable, and comparable on the basis of the protocol described earlier (Weber et al, 2015).

The effect of lymphatic deficiency after a single antigen exposition has not been extensively characterized earlier. When single antigen treatment was administered, we detected an increased thickening of the lymphatic-deficient ears compared with that observed in the ears with intact lymphatics, but no significant difference in the immune cell infiltration and local cytokine release was observed (Supplementary Figures S4 and S5). This suggests a tendency toward local edema formation in the treated skin in our models lacking skin lymphatics, which however was not followed by a considerable inflammatory response after single antigen exposure.

It has been well-characterized earlier that lymphatics serve as a highway for immune cells, including professional antigen-presenting cells, to migrate to the local lymph nodes. However, the importance of the lymphatics in the initiation of the sensitization phase of CHS has not been extensively studied (Collado-Diaz et al, 2022). In this study, we showed that the absence of lymphatics in the sensitization phase results in a less pronounced immune response, suggesting that the lymphatics-dependent mechanisms are critical for effective induction of the pathogenesis of CHS during the sensitization phase (Figures 2–4). In contrast, the inflammatory response was much more robust when lymphatics were absent in the elicitation phase, showing that the immunomodulatory effect of lymphatics is primarily detectable after the repeated antigen challenge (Figure 5). Blockade of VEGFR3 signaling using an antibody-mediated strategy in an acute manner in CHS also resulted in an accelerated immune response (Huggenberger et al, 2010; Schwager and Detmar, 2019). Other findings using similar experimental strategies with VEGFR3-blocking antibodies indicated increased inflammation in inflammatory bowel disease and transgenic TNF mouse model of rheumatoid arthritis (D'Alessio et al, 2014; Guo et al, 2009; Jurisic et al, 2013; Schwager and Detmar, 2019). It is important to note that the application of a VEGFR3-blocking antibody is not directly comparable with an experimental model in which lymphatics are absent in the skin, as utilized in this study. Even though both strategies can modulate the immune response, the mechanism of their effect may be quite different. In addition, acute and/or uncontrolled effects of the VEGF-C–VEGFR3 axis stimulation in disease models with adenovirus and transgenic strategies also have inherent limitations. Moreover, not only lymphatics but other cell types, including immune cells, can be influenced by these strategies. Of note, mostly, these approaches were used before to understand the role of skin lymphatics in CHS and other inflammatory diseases (Huggenberger and Detmar, 2011; Huggenberger et al, 2011, 2010; Kataru et al, 2009; Schwager and Detmar, 2019). In connection, the VEGF-C–VEGFR3 axis acts as an important therapeutic target in inflammatory diseases (Cousin et al, 2022; Schwager et al, 2018). Because our results describe a more robust inflammatory reaction in the elicitation phase of CHS in the absence of lymphatics, they align with previous reports indicating a more challenging management of patients with the combination of allergic contact dermatitis and lymphedema (Dyring-Andersen et al, 2011).

Both TNCB and DNFB were effective to induce CHS; however, the more pronounced swelling of the ear of the lymphatic-deficient mice compared to the mice with intact lymphatics was not present when repeated DNFB was used (Supplementary Figure S3c), whereas an increased $CD45^+$ cell infiltration was observed still, suggesting that the local inflammatory processes are hapten dependent (Supplementary Figure S3d).

It has been known that the neutrophil granulocytes are key players both in the sensitization and elicitation phases of CHS (Weber et al, 2015), but the exact mechanisms of how neutrophils influence inflammation in collaboration with

Wilcoxon signed-rank test; mean ± SEM; n = 7 for each group). **(e)** CD45-expressing cells are shown in ear sections by fluorescent immunohistology. Bars = 50 μm; n = 6 for each group. Number of $CD45^+$ cells quantified on the basis of fluorescent immunohistology ($P = .0156$; 2-tailed, paired *t*-test; mean ± SEM; n = 4 for each group). **(f)** Same as **e** for GR1-expressing cells. Bars = 50 μm; n = 6 for each group. Quantification of $GR1^+$ cell numbers based on fluorescent immunohistology ($P = .0125$, 2-tailed, paired *t*-test; mean ± SEM; n = 4 for each group). **(g)** The effect of the second antigen exposure on immune cell counts from ears at days 6 and 9 (day 6: $P = .0471$ for $CD45^+$ cells, and $P = .9574$ for $B220^+$ cells; 2-tailed, paired *t*-test; mean ± SEM; n = 9 and n = 10 for the groups with intact lymphatics and lymphatic deficiency; $P = .0039$ for $Ly6G^+$ cells and $P = .1641$ for $CD3^+$ cells; Wilcoxon signed-rank test; mean ± SEM; n = 9 for each group; day 9 measured by CytoFLEX: $P = .0176$ for $CD45^+$ cells, 2-tailed, unpaired *t*-test; $P = .0317$ for $Ly6G^+$ cells, Mann–Whitney *U* test; mean ± SEM; n = 5 for each group). **(h)** Cytokine array to detect cytokine expression in ear tissue supernatants. The representative images show the arrangement of the cytokines in duplicates (n = 3 from each group). Data are shown from a 10-minute exposure to the X-ray film containing our experimental groups. **(i)** Summary graph of the quantification of the cytokine array demonstrating the effect of the second antigen exposure over the first (2-tailed, paired *t*-test; mean ± SEM; n = 3 for each group). DT, diphtheria toxin; ns, not significant; RS reference spot.

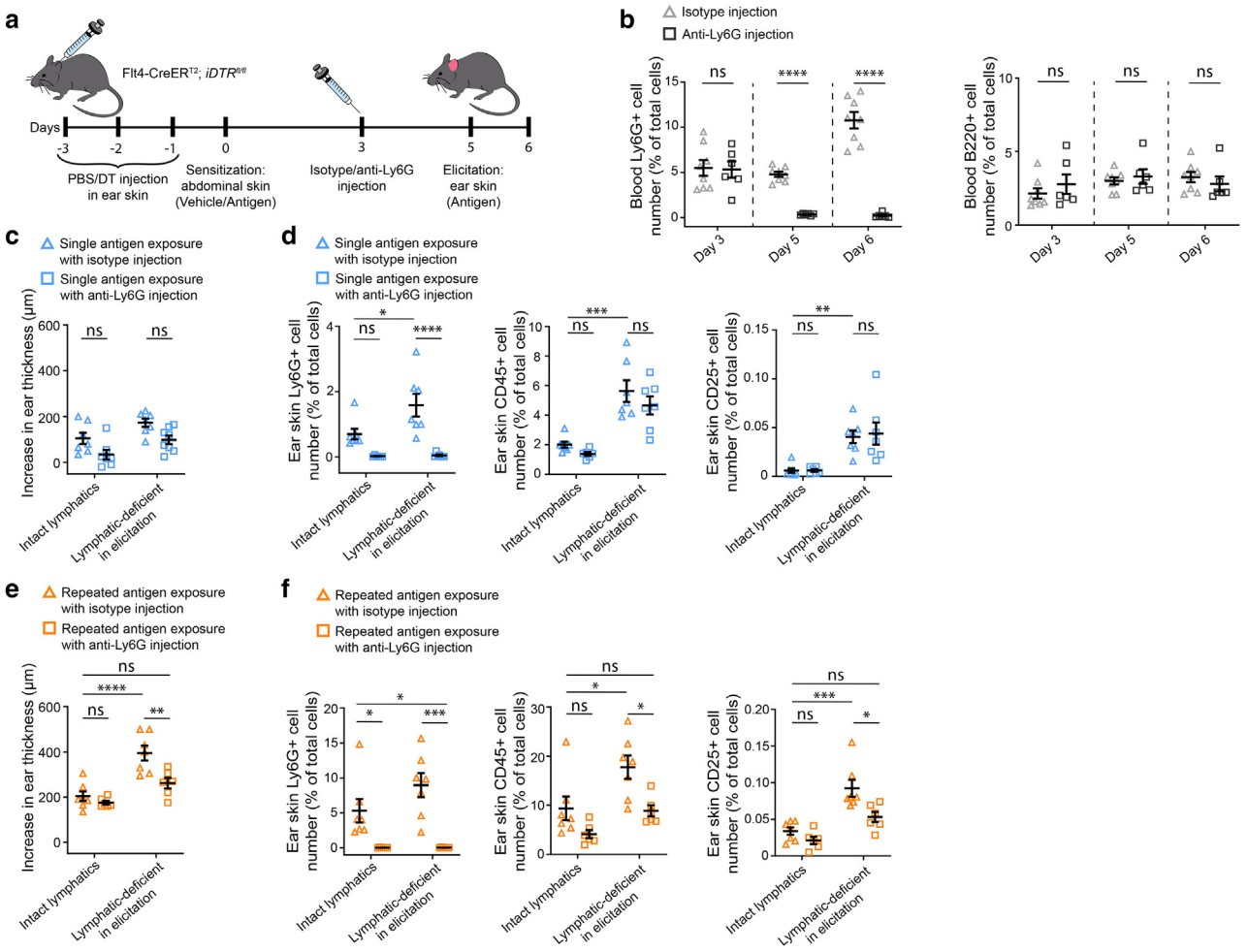

Figure 6. The effect of neutrophil granulocyte depletion in elicitation phase of CHS in the absence of lymphatics. **(a)** Flt4-CreER^{T2}; *iDTR*$^{fl/fl}$ mice were injected with PBS or DT into the ear skin for 3 days. Three days after the first injection, mice with intact lymphatics or local lymphatic deficiency in ear (marked with pink color) were treated with vehicle or antigen on the abdominal skin. Five days after exposure, antigen treatment was repeated on ear skin. Two days before the elicitation, the mice received anti-Ly6G injection to eliminate neutrophil granulocytes or IgG isotype injection as a control. **(b)** Ly6G$^+$ and B220$^+$ immune cell numbers in peripheral blood before and after neutrophil depletion measured by CytoFLEX (Ly6G: $P = .90135$ for day 3; $P < .00001$ for day 5; $P < .00001$ for day 6; B220: $P = .38774$ for day 3; $P = .55165$ for day 5; $P = .46292$ for day 6; 2-tailed, unpaired *t*-test; mean ± SEM; n = 8 and n = 7 for the groups with isotype control and anti-Ly6G injection, respectively). **(c)** The increase in ear thickness of mice with intact lymphatics and lymphatic-deficient mice in elicitation phase followed by neutrophil depletion after single exposure (2-way ANOVA with Tukey's multiple comparisons test; mean ± SEM; n = 8 for the group with lymphatic deficiency after neutrophil depletion and n = 7 for the remaining group; normal lymphatics with isotype injection vs neutrophil depletion: $P = .1022$; lymphatic deficiency with isotype injection vs neutrophil depletion: $P = .0690$). **(d)** Ly6G$^+$, CD45$^+$, and CD25$^+$ immune cell numbers after single antigen exposure measured by CytoFLEX (2-way ANOVA with Tukey's multiple comparisons test; mean ± SEM; n = 7 for each group; Ly6G: normal lymphatics with isotype injection vs neutrophil depletion: $P = .1195$; lymphatic deficiency with isotype injection vs neutrophil depletion: $P < .0001$; normal lymphatics vs lymphatic deficiency with isotype injection: $P = .0199$; CD45: normal lymphatics with isotype injection vs neutrophil depletion: $P = .8285$; lymphatic deficiency after single exposure with isotype injection vs neutrophil depletion: $P = .5319$; normal lymphatics vs lymphatic deficiency with isotype injection: $P = .0002$; CD25: normal lymphatics with isotype injection vs neutrophil depletion: $P > .9999$; normal lymphatics vs lymphatic deficiency with isotype injection: $P = .0053$; lymphatic deficiency with isotype injection vs neutrophil depletion: $P = .9849$; normal lymphatics vs lymphatic deficiency with isotype injection: $P = .0081$). **(e)** The increase in ear thickness of mice with intact lymphatics and lymphatic-deficient mice in elicitation phase followed by neutrophil depletion after repeated exposure (2-way ANOVA with Tukey's multiple comparisons test; mean ± SEM; n = 7 and n = 6 for the groups with isotype injection and neutrophil depletion, respectively; normal lymphatics with isotype injection vs neutrophil depletion: $P = .8482$; lymphatic deficiency with isotype injection vs neutrophil depletion: $P = .0042$; normal lymphatics with isotype injection vs lymphatic deficiency with neutrophil depletion: $P = .3472$; normal lymphatics vs lymphatic deficiency with isotype injection: $P < .0001$). **(f)** Ly6G$^+$, CD45$^+$, and CD25$^+$ immune cell numbers after single repeated exposure measured by CytoFLEX (2-way ANOVA with Tukey's multiple comparisons test; mean ± SEM; n = 7 for each group; Ly6G: normal lymphatics with isotype injection vs neutrophil depletion: $P = .0431$; lymphatic deficiency with isotype injection vs neutrophil depletion: $P = .0004$; normal lymphatics with isotype injection vs lymphatic deficiency with neutrophil depletion after repeated exposure: $P = .0433$; CD45: normal lymphatics with isotype injection vs neutrophil depletion: $P = .2583$; lymphatic deficiency with isotype injection vs neutrophil depletion: $P = .0186$; normal lymphatics vs lymphatic deficiency with isotype injection: $P = .0213$; normal lymphatics with isotype injection vs lymphatic deficiency with neutrophil depletion after repeated exposure: $P = .9977$; CD25: normal lymphatics with isotype injection vs neutrophil depletion: $P = .6791$; lymphatic deficiency with isotype injection vs neutrophil depletion: $P = .0103$; normal lymphatics vs lymphatic deficiency with isotype injection: $P = .0001$; normal lymphatics with isotype injection vs lymphatic deficiency with neutrophil depletion after repeated exposure: $P = .3332$). CHS, contact hypersensitivity; DT, diphtheria toxin; ns, not significant.

lymphatics remained unclear. Our results now demonstrate the critical involvement of neutrophil granulocytes in driving the exaggerated immune response in the absence of lymphatics, significantly impacting the recruitment of regulatory T cells (Figure 6). Regulatory T cell trafficking between lymph nodes and the inflamed tissue is essential for optimal immune suppression (Rudensky and Campbell, 2006). However, the regulatory T cell-homing and recirculation may be impaired owing to the lack of interaction with lymphatic endothelial cells during acute inflammation (Piao et al, 2020). Previous studies have shown that regulatory T cells engage in complex crosstalk with neutrophils (Ou et al, 2023), but further investigations are needed to better understand their role in the context of the lymphatic system.

In summary, we described the involvement of skin lymphatic density in the progression of CHS using genetic mouse models lacking lymphatics in only the sensitization or elicitation or in both phases of CHS. Our experimental data suggest that lymphatics modulate both phases of CHS: in the sensitization phase, lymphatics contribute to the development of the antigen-induced immunization, whereas in the elicitation phase, these structures moderate the inflammatory response and immune cell infiltration. Our results indicate that different strategies are needed during the 2 phases of CHS to modulate the progression of the disease.

MATHERIALS AND METHODS

Experimental animals

Wild-type mice and mice carrying an *Flt4* kinase-dead allele on NMRI genetic background aged 8–16 weeks were used for the experiments ($Flt4^{kd/+}$, also named as $Vegfr3^{kd/+}$; MRC Harwell) (Karkkainen et al, 2001). The mice were genotyped by allele-specific PCR reaction from tail DNA samples using 5′ – CTA GCT GAG TCC CTA ACT CG – 3′ forward and 5′ – CGG GGT CTT TGT AGA TGT CC – 3′ reverse primers. To detect the mutation of the kinase-dead allele, the PCR product was digested by BGL II enzyme (Life Technologies).

To delete lymphatics locally in the skin of a transgenic inducible lymphatic vessel elimination model, the Flt4-CreER^{T2}, $iDTR^{fl/fl}$ strain (on C57Bl/6 background) was used (Buch et al, 2005; Gardenier et al, 2016; Martinez-Corral et al, 2016). The strain was maintained in homozygous form. Allele-specific PCR using Flt4-CreER^{T2} knock-in–specific forward (5′ – GGC TGG ACC AAT GTA AAT ATT G – 3′) and reverse (5′ – CAT CAT CGA AGC TTCA CTG – 3′), *Flt4* wild-type specific forward (5′ – CAC TAT GCT CCG TGT CTT G -3′) and reverse (5′ – GTG ACT CTC AGA CAT ATG – 3′), and $iDTR^{fl/fl}$ allele–specific reverse (5′– CAT CAA GGA AAC CCT GGA CTA CTG – 3′) and common forward (5′ – AAA GTC GCT CTG AGT TGT TAT – 3′) and wild-type site specific reverse (5′ – GGA GCG GGA GAA ATG GAT ATG – 3′) primers were used to confirm genotypes.

To visualize the lymphatic vessels in $Flt4^{kd/+}$and the Flt4-CreER^{T2}; $iDTR^{fl/+}$ mice, these strains were crossed with the $Prox1^{GFP}$ lymphatic reporter mice (Choi et al, 2011) (maintained on C57Bl/6 background). The allele-specific genotyping was based on the forward 5′ – GAT GTG CCA TAA ATC CCA GAG CCT AT – 3′ and reverse 5′– GGT CGG GGT AGC GGC TGA A – 3′ primers.

All animal experiments were approved by the Animal Experimentation Review Board of the Semmelweis University and the Government Office for Pest County (license numbers of ethic votes: PE/EA/148-4/2018, PE/EA/1654-7/2018, PE/EA/00658-6/2023, and PE/EA/00659-6/2023). Experimental animals were housed in either specific pathogen-free or conventional animal facilities between 18–22 °C, 45% humidity, and 12/12 hours dark–light cycles. Food and the water were supplied ad libitum.

Inducible lymphatic vessel elimination mouse model

The Flt4-CreER^{T2}; $iDTR^{fl/fl}$ transgenic mouse model was used to eliminate the lymphatic vessels locally in a tamoxifen-dependent manner as described before (Szőke et al, 2021). Tamoxifen (Sigma-Aldrich) was dissolved at a concentration of 20 mg/ml in corn oil (Sigma-Aldrich), and 4.5 mg/40 g body weight dose of tamoxifen was injected intraperitoneally to adult Flt4-CreER^{T2}, $iDTR^{fl/fl}$ and $Prox1^{GFP}$; Flt4-CreER^{T2}; $iDTR^{fl/+}$ mice once daily for 5 consecutive days. One week after the last tamoxifen treatment, 60 ng DT (Sigma-Aldrich, D0564) dissolved in 30 μl PBS was injected once daily for 3 days either into the hind limb (to ablate the lymphatics specifically during sensitization phase) or into the right ear (to ablate the lymphatics specifically during elicitation phase). As a control, PBS was administered into the contralateral ear of the same mice or into the hind paw of a littermate.

CHS model

Isoflurane (Baxter) was used to anaesthetize the mice during the treatment. Mouse CHS model induction was based on the protocol described before (Weber et al, 2015).

Single antigen exposure. In the sensitization phase, the mice were treated with 100 μl acetone as a vehicle control on the shaved abdominal skin of the $Vegfr3^{+/+}$ and $Vegfr3^{kd/+}$ mice (lacking lymphatics both in the sensitization and the elicitation phases) and on the shaved abdominal skin of Flt4-CreER^{T2}, $iDTR^{fl/fl}$ mice (after the administration of PBS and DT into the ear of the mouse labeled as lacking lymphatics in the elicitation phase) and on the hind paw skin of Flt4-CreER^{T2}, $iDTR^{fl/fl}$ mice (after the administration of PBS or DT into the hind paw of the mouse labeled as lacking lymphatics in the sensitization phase). After 5 days, the initial ear thickness of mice was measured using a caliper (Käfer Messuhrenfabrik GmbH). For elicitation, mice were treated on both ears by epicutaneous application of 20 μl 1% TNCB (Sigma-Aldrich, 79874) diluted in acetone. A total of 20 μl of acetone on ear skin was also applied as an absolute control group. Twenty-four hours after the challenge, the ear swelling was measured again. The increase in ear thickness was assessed as the difference between the values prior and 24 hours after the challenge, indicated by blue coloring in the graphs.

Repeated antigen exposure. In the sensitization phase, the abdominal skin or hind paw skin of mice was treated with 100 μl 3% TNCB diluted in acetone as an antigen, as detailed earleir. Five days after sensitization, the initial ear thickness was measured using a caliper. For elicitation, mice were treated on both ears by epicutaneous application of 20 μl 1% TNCB diluted in acetone as a second exposure of antigen. The ear swelling was determined as described earlier, indicated by orange coloring in the graphs. To investigate the specificity of the antigen, DNFB (Sigma-Aldrich, D1529) was used as a different hapten during the CHS model.

Neutrophil depletion. Flt4-CreER^{T2}, $iDTR^{fl/fl}$ mice were treated with tamoxifen followed by DT or PBS injection in the ear skin as described ealier. The mice were then sensitized on abdominal skin with 100 μl 3% TNCB diluted in acetone as an antigen or 100 μl of acetone as a control, as detailed earlier. Three days after the

sensitization, mice were intraperitoneally injected with 100 μg of murinized anti-Ly6G antibody (Absolute Antibody, Ab00295-2.0) to deplete neutrophil granulocytes or with 100 μg of functional grade IgG2a kappa isotype antibody (Invitrogen, 16-4724-85) serving as control. Elicitation on ear skin was performed 2 days after the injection, as described earlier. The success of the depletion of neutrophils (labeled as $Ly6G^+$ cells) was confirmed with flow cytometry from peripheral blood samples using anti-Ly6G PerCP-Cy5.5 (BD Biosciences, 560602), anti-CD11b-allophycocyanin (BD Biosciences, 553312) and anti-CD45-FITC (Biolegend, 103108) staining, also considering the characteristic population in the forward scatter-side scatter plot.

Restimulation of lymph node cells (passive CHS model)

The hind paw of Flt4-$CreER^{T2}$, *iDTR*$^{fl/fl}$ mice were injected with PBS or DT once daily for 3 days after tamoxifen treatment. Eight days after the first DT injection, the hind paw skin was treated with 100 μl acetone or 3% TNCB in acetone for the sensitization. Five days after sensitization, the regional lymph nodes were collected, and single-cell suspension was prepared by homogenizing the inguinal lymph nodes through a 70-μm cell strainer using the hard end of a syringe plunger. For activation, the cells were incubated with PBS as a control or with 3 mM solution of TNBS (2,4,6-trinitrobenzenesulfonic acid — water soluble form of TNCB; Sigma-Aldrich, P2297) for 7 minutes at 37 °C in the dark. After washing steps, 10^6 cells were incubated in RPMI medium (contains glutamine, 10% fetal bovine serum, penicillin, streptavidin) in a 96-well plate for 48 hours. After that, the supernatant was collected, and IFN-γ production was measured by ELISA (Thermo Fisher Scientific, BMS606TWO), according to the manufacturer's instructions.

Histological procedures and immunostaining

Isolated tissues (ear, back skin, small intestine, lung) were fixed in 4% paraformaldehyde (Sigma-Aldrich) overnight at 4 °C, dehydrated in a series of ethanol solutions (50, 70, 95, and 100% concentration), and embedded into paraffin (Leica) using a Leica EG1150H embedding station. A total of 7–8-μm-thick sections were produced using a Thermo Scientific microtome (HM340E) and were processed for H&E (Leica) staining and different types of fluorescent immunostainings. The immunostainings were performed using the following antibodies in 1:50 dilution incubating at 4 °C overnight: anti-LYVE1 (R&D Systems, AF2125), anti-CD31 (R&D Systems, mab3628), anti-Ly6G/Ly6C (anti-GR1) (BD Biosciences, 550291, clone RB6-8C5), anti-CD45 (clone IBL-5/25), anti-PDPN (BioLegend, 127402), and anti-GFP (Life Technologies, A11122). The secondary antibodies conjugated with fluorophores (Life Technologies) were diluted in 1:250, incubating at room temperature for 1 hour: Alexa Fluor 488 goat anti-rabbit IgG (A11034), Alexa Fluor 488 donkey anti-goat IgG (A11055), Alexa Fluor 568 donkey anti-goat IgG (A11057), Alexa Fluor 488 donkey anti-rat IgG (A21208), Alexa Fluor 594 donkey anti-rat IgG (A21209), and Alexa Fluor 594 donkey anti-hamster IgG (A21113). As a nuclear staining, DAPI containing mounting medium (Vector Laboratories, H-1200) was used. Microscopic images were taken by a Nikon ECLIPSE Ni-U microscope connected to a Nikon DS-Ri2 camera.

The ankles were collected from mice after injection with PBS or DT and were fixed in 4% paraformaldehyde at 4 °C for 4 days. After 2-day-long PBS washing steps, samples were decalcified in Osteomoll (Merck) for 3 weeks. The samples were dehydrated, embedded, and sectioned as described earlier.

Lymphatic vessel number and area (mean of all visible lymphatic vessels in 1 mouse ear section) were quantified in NIS-Elements Imaging Software (Nikon) from anti-LYVE1 fluorescent immunostained images taken with a ×20 objective. Blood vessel numbers (average of 3 fields of view per tissue section) were quantified in NIS-Elements Imaging Software (Nikon) from anti-CD31 and anti-LYVE1 fluorescent immunostained images taken with a ×20 objective. Number of $CD45^+$ and $GR1^+$ immune cells were counted in FIJI Software (version 1.53q) (Schindelin et al, 2012) using anti-CD45 and anti-GR1 fluorescent immunohistology images (average of 2 fields of view per tissue section).

Whole mount immunostaining

The 4% paraformaldehyde–fixed ears were blocked and then were incubated with anti-LYVE1 primary antibody in 1:150 dilution at 4 °C overnight followed by anti-goat secondary antibody conjugated to Alexa Fluor 488 in 1:150 dilution. Fluorescence stereo microscopic images were taken using a Nikon SMZ25 microscope connected to a Nikon DS-Ri2 camera.

Digestion of skin samples

Ear skin was collected and cut into small pieces. The samples were digested with Liberase II kit (Roche, 492430) in a microtube Thermo-Shaker (BioSan TS-100) for 1 hour at 37 °C and at 1400 r.p.m. Alternatively, ear skin samples were digested in a solution of 2.5 mg/ml Collagenase D (Roche, 1108888201) and 10 mg/ml DNase I (Roche, 11284932001) dissolved in RPMI (containing glutamine, 10% fetal bovine serum, penicillin, streptavidin) in a microtube Thermo-Shaker (BioSan TS-100) for 30 minutes at 37 °C and at 250 r.p.m. Single-cell suspension was prepared by passing through a 70-μm cell strainer (Falcon). The supernatant was collected for mouse cytokine array.

Mouse cytokine array panel A

The tissue supernatants from the mouse ear samples were prepared as described in the Digestion of skin samples section. A total of 500 μl of the supernatant was run on the array as described in the kit protocol (R&D Systems, ARY006). Representative images are shown of our experimental groups from a 5–10-minute exposure to the same X-ray film. The pixel intensity of dots on X-ray film was evaluated by FIJI Software (version 1.51n) (Schindelin et al, 2012).

Flow cytometry

Single cell suspension prepared as described earlier was stained with anti-CD45-phycoeryhtrin (BD Biosciences, 553081) and anti-Ly6G-PerCP-Cy5.5 (BD Biosciences, 560602) or anti-CD45R/B220-phycoeryhtrin (BD Biosciences, 553090) and anti-CD3-Alexa Fluor 647 (BD Biosciences, 557869) in a 1:200 dilution of PBS-based buffer containing 2% heparin and 5% heat inactivated fetal bovine serum. The conjugated primary antibody incubation was carried out for 1 hour at 4 °C. After staining, the samples were analyzed by BD Biosciences FACSCalibur cytometer.

Alternatively, the single-cell suspension was stained with anti-CD45-FITC (BioLegend, 103108), anti-CD45R/B220-phycoeryhtrin (BD Biosciences, 553090), anti-Ly6G-PerCP-Cy5.5 (BD Biosciences, 560602), anti-CD25-allophycocyanin (Invitrogen, 17-0251-82), anti-CD279 (PD-1)-allophycocyanin/Fire 750 (BioLegend, 135240), anti-CD3-phycoeryhtrin/cyanine 7 (BioLegend, 100220), anti-CD8a-Pacific Blue (Invitrogen, MCD0828), and anti-CD4-Pacific Orange (Invitrogen, MCD0430) in a 1:200 dilution of PBS-based buffer containing 2% heparin and 5% heat-inactivated fetal bovine serum. The conjugated primary antibody incubation was carried out for 1 hour at

4 °C. After washing, pellets were dissolved in PBS and were analyzed by a Beckman Coulter CytoFLEX cytometer.

Presentation of data and statistical analysis

Microscopic image processing and analysis were performed using Nikon NIS-Elements Imaging Software, Adobe Illustrator, and Adobe Photoshop. Flow cytometry data were evaluated using FCS express or CytExpert software. Experiments were performed the number of times indicated in the figure legends. Bar graphs show the mean and SEM of all mice or samples from indicated number of independent experiments. The effect of the second antigen exposure in ear thickness/immune cell infiltration/cytokine expression is calculated by subtracting the mean of the corresponding control group after single antigen exposure from the individual data points after repeated exposure, indicated by purple coloring in the graphs. Statistical analysis was performed in GraphPad Prism 7.0 and Excel 2018. Normal distribution of all datasets was assessed using the Shapiro–Wilk test. The significance of difference between groups was assessed by paired or unpaired Student's *t*-test, Mann–Whitney *U* test, Wilcoxon signed-rank test, or 2-way ANOVA. An $\alpha < 0.05$ was considered statistically significant, showing $^{*}P < .05$, $^{**}P < .01$, $^{***}P < .001$, and $^{****}P < .0001$.

DATA AVAILABILITY STATEMENT

All the data supporting the findings of this study are available within the article and from the corresponding author upon reasonable request.

ORCIDs

Petra Aradi: http://orcid.org/0009-0003-0854-1311
Gabor Kovacs: http://orcid.org/0000-0002-6279-5131
Eva Kemecsei: http://orcid.org/0000-0002-3602-7112
Kornel Molnar: http://orcid.org/0009-0000-4944-1980
Stella Marta Sagi: http://orcid.org/0009-0003-3228-2655
Zalan Horvath: http://orcid.org/0009-0009-6117-8527
Babak J. Mehrara: http://orcid.org/0000-0001-5717-697X
Raghu P. Kataru: http://orcid.org/0000-0003-1315-7982
Zoltan Jakus: http://orcid.org/0000-0002-6304-2369

CONFLICT OF INTEREST

The authors state no conflict of interest.

ACKNOWLEDGMENTS

We thank V. Németh, E. Marinkás, and D. Csengel for excellent technical assistance, Tomer Zilbermintz for help with experiments and Young-Kwon Hong for *Prox1*^{GFP} mice. This work was supported by the National Research, Development and Innovation Office (K139165, TKP2021-EGA-29, TKP2021-EGA-24, NVKP_16-1-2016-0039), the European Union and the Hungarian Government (VEKOP-2.3.2-16-2016-00002, VEKOP-2.3.3-15-2016-00006, EFOP-3.6.3-VEKOP-16-2017-00009). ZJ is a recipient of the János Bolyai Research Scholarship of the Hungarian Academy of Sciences (BO/00898/22) and the New National Excellence Program of the Ministry for Culture and Innovation from the source of the National Research, Development and Innovation Fund (UNKP-23-5-SE-10). KM was supported by the National Academy of Scientist Education Program of the National Biomedical Foundation. ZJ dedicates this work to the memory of his father.

AUTHOR CONTRIBUTIONS

Conceptualization: PA, GK, ZJ; Formal Analysis: PA, GK, EK, KM, SMS, ZH, ZJ; Funding Acquisition: ZJ; Investigation: PA, GK, EK, KM, SMS, ZH, ZJ; Methodology: PA, GK, EK, BJM, RPK, ZJ; Project Administration: ZJ; Supervision: ZJ; Visualization: PA, GK; Writing – Original Draft Preparation: PA, GK, ZJ; Writing – Review and Editing: EK, KM, SMS, ZH, BJM, RPK

SUPPLEMENTARY MATERIAL

Supplementary material is linked to the online version of the paper at www.jidonline.org, and at https://doi.org/10.1016/j.jid.2024.03.021.

REFERENCES

Azeem M, Kader H, Kerstan A, Hetta HF, Serfling E, Goebeler M, et al. Intricate relationship between adaptive and innate immune system in allergic contact dermatitis. Yale J Biol Med 2020;93:699–709.

Buch T, Heppner FL, Tertilt C, Heinen TJ, Kremer M, Wunderlich FT, et al. A Cre-inducible diphtheria toxin receptor mediates cell lineage ablation after toxin administration. Nat Methods 2005;2:419–26.

Choi I, Chung HK, Ramu S, Lee HN, Kim KE, Lee S, et al. Visualization of lymphatic vessels by Prox1-promoter directed GFP reporter in a bacterial artificial chromosome-based transgenic mouse. Blood 2011;117:362–5.

Christ C, Jakus Z. Visualization of organ-specific lymphatic growth: an efficient approach to labeling molecular markers in cleared tissues. Int J Mol Sci 2023;24:5075.

Collado-Diaz V, Medina-Sanchez JD, Gkountidi AO, Halin C. Imaging leukocyte migration through afferent lymphatics. Immunol Rev 2022;306:43–57.

Cousin N, Bartel S, Scholl J, Tacconi C, Egger A, Thorhallsdottir G, et al. Antibody-mediated delivery of VEGF-C promotes long-lasting lymphatic expansion that reduces recurrent inflammation. Cells 2022;12:172.

D'Alessio S, Correale C, Tacconi C, Gandelli A, Pietrogrande G, Vetrano S, et al. VEGF-C-dependent stimulation of lymphatic function ameliorates experimental inflammatory bowel disease. J Clin Invest 2014;124:3863–78.

Dyring-Andersen B, Skov L, Jensen P. Chronic lymphoedema caused by recurrent infections in a patient with allergic hand eczema. Dermatol Reports 2011;3:e11.

Gardenier JC, Hespe GE, Kataru RP, Savetsky IL, Torrisi JS, Nores GDG, et al. Diphtheria toxin-mediated ablation of lymphatic endothelial cells results in progressive lymphedema. JCI Insight 2016;1:e84095.

Guo R, Zhou Q, Proulx ST, Wood R, Ji RC, Ritchlin CT, et al. Inhibition of lymphangiogenesis and lymphatic drainage via vascular endothelial growth factor receptor 3 blockade increases the severity of inflammation in a mouse model of chronic inflammatory arthritis. Arthritis Rheum 2009;60:2666–76.

Hagura A, Asai J, Maruyama K, Takenaka H, Kinoshita S, Katoh N. The VEGF-C/VEGFR3 signaling pathway contributes to resolving chronic skin inflammation by activating lymphatic vessel function. J Dermatol Sci 2014;73:135–41.

Honda T, Egawa G, Grabbe S, Kabashima K. Update of immune events in the murine contact hypersensitivity model: toward the understanding of allergic contact dermatitis. J Invest Dermatol 2013;133:303–15.

Honda T, Egawa G, Kabashima K. Antigen presentation and adaptive immune responses in skin. Int Immunol 2019;31:423–9.

Huggenberger R, Detmar M. The cutaneous vascular system in chronic skin inflammation. J Investig Dermatol Symp Proc 2011;15:24–32.

Huggenberger R, Siddiqui SS, Brander D, Ullmann S, Zimmermann K, Antsiferova M, et al. An important role of lymphatic vessel activation in limiting acute inflammation. Blood 2011;117:4667–78.

Huggenberger R, Ullmann S, Proulx ST, Pytowski B, Alitalo K, Detmar M. Stimulation of lymphangiogenesis via VEGFR-3 inhibits chronic skin inflammation. J Exp Med 2010;207:2255–69.

Jurisic G, Sundberg JP, Detmar M. Blockade of VEGF receptor-3 aggravates inflammatory bowel disease and lymphatic vessel enlargement. Inflamm Bowel Dis 2013;19:1983–9.

Kabashima K, Honda T, Ginhoux F, Egawa G. The immunological anatomy of the skin. Nat Rev Immunol 2019;19:19–30.

Kaipainen A, Korhonen J, Mustonen T, van Hinsbergh VW, Fang GH, Dumont D, et al. Expression of the fms-like tyrosine kinase 4 gene becomes restricted to lymphatic endothelium during development. Proc Natl Acad Sci U S A 1995;92:3566–70.

Kaplan DH, Igyártó BZ, Gaspari AA. Early immune events in the induction of allergic contact dermatitis. Nat Rev Immunol 2012;12:114–24.

Karkkainen MJ, Saaristo A, Jussila L, Karila KA, Lawrence EC, Pajusola K, et al. A model for gene therapy of human hereditary lymphedema. Proc Natl Acad Sci U S A 2001;98:12677–82.

Kataru RP, Baik JE, Park HJ, Wiser I, Rehal S, Shin JY, et al. Regulation of immune function by the lymphatic system in lymphedema. Front Immunol 2019;10:470.

Kataru RP, Jung K, Jang C, Yang H, Schwendener RA, Baik JE, et al. Critical role of CD11b+ macrophages and VEGF in inflammatory lymphangiogenesis, antigen clearance, and inflammation resolution. Blood 2009;113:5650–9.

Manresa MC. Animal models of contact dermatitis: 2,4-dinitrofluorobenzene-induced contact hypersensitivity. Methods Mol Biol 2021;2223:87–100.

Martin SF. Immunological mechanisms in allergic contact dermatitis. Curr Opin Allergy Clin Immunol 2015;15:124–30.

Martin SF, Esser PR, Weber FC, Jakob T, Freudenberg MA, Schmidt M, et al. Mechanisms of chemical-induced innate immunity in allergic contact dermatitis. Allergy 2011;66:1152–63.

Martinez-Corral I, Stanczuk L, Frye M, Ulvmar MH, Diéguez-Hurtado R, Olmeda D, et al. Vegfr3-CreER (T2) mouse, a new genetic tool for targeting the lymphatic system [published correction appears in Angiogenesis 2016;19:447]. Angiogenesis 2016;19:433–45.

Novak-Bilić G, Vučić M, Japundžić I, Meštrović-Štefekov J, Stanić-Duktaj S, Lugović-Mihić L. Irritant and allergic contact dermatitis - skin lesion characteristics. Acta Clin Croat 2018;57:713–20.

Oliver G, Kipnis J, Randolph GJ, Harvey NL. The lymphatic Vasculature in the 21st Century: novel functional roles in homeostasis and disease. Cell 2020;182:270–96.

Ou Q, Power R, Griffin MD. Revisiting regulatory T cells as modulators of innate immune response and inflammatory diseases. Front Immunol 2023;14:1287465.

Piao W, Xiong Y, Li L, Saxena V, Smith KD, Hippen KL, et al. Regulatory T cells condition lymphatic endothelia for enhanced transendothelial migration. Cell Rep 2020;30:1052–62.e5.

Prop J, Griffiths A, Hutchinson IV, Morris PJ. Specific suppressor T cells in rats active in the afferent phase of contact hypersensitivity. Cell Immunol 1986;99:73–84.

Rauniyar K, Jha SK, Jeltsch M. Biology of vascular endothelial growth factor C in the morphogenesis of lymphatic vessels. Front Bioeng Biotechnol 2018;6:7.

Rudensky AY, Campbell DJ. In vivo sites and cellular mechanisms of T reg cell-mediated suppression. J Exp Med 2006;203:489–92.

Scheinman PL, Vocanson M, Thyssen JP, Johansen JD, Nixon RL, Dear K, et al. Contact dermatitis. Nat Rev Dis Primers 2021;7:38.

Schindelin J, Arganda-Carreras I, Frise E, Kaynig V, Longair M, Pietzsch T, et al. Fiji: an open-source platform for biological-image analysis. Nat Methods 2012;9:676–82.

Schwager S, Detmar M. Inflammation and lymphatic function. Front Immunol 2019;10:308.

Schwager S, Renner S, Hemmerle T, Karaman S, Proulx ST, Fetz R, et al. Antibody-mediated delivery of VEGF-C potently reduces chronic skin inflammation. JCI Insight 2018;3:e124850.

Strzepa A, Gurski CJ, Dittel LJ, Szczepanik M, Pritchard KA Jr, Dittel BN. Neutrophil-derived myeloperoxidase facilitates both the induction and elicitation phases of contact hypersensitivity. Front Immunol 2020;11:608871.

Szőke D, Kovács G, Kemecsei É, Bálint L, Szoták-Ajtay K, Aradi P, et al. Nucleoside-modified VEGFC mRNA induces organ-specific lymphatic growth and reverses experimental lymphedema. Nat Commun 2021;12:3460.

Tammela T, Alitalo K. Lymphangiogenesis: molecular mechanisms and future promise. Cell 2010;140:460–76.

Vocanson M, Hennino A, Rozières A, Poyet G, Nicolas JF. Effector and regulatory mechanisms in allergic contact dermatitis. Allergy 2009;64:1699–714.

Weber FC, Németh T, Csepregi JZ, Dudeck A, Roers A, Ozsvári B, et al. Neutrophils are required for both the sensitization and elicitation phase of contact hypersensitivity. J Exp Med 2015;212:15–22.

Worbs T, Hammerschmidt SI, Förster R. Dendritic cell migration in health and disease. Nat Rev Immunol 2017;17:30–48.

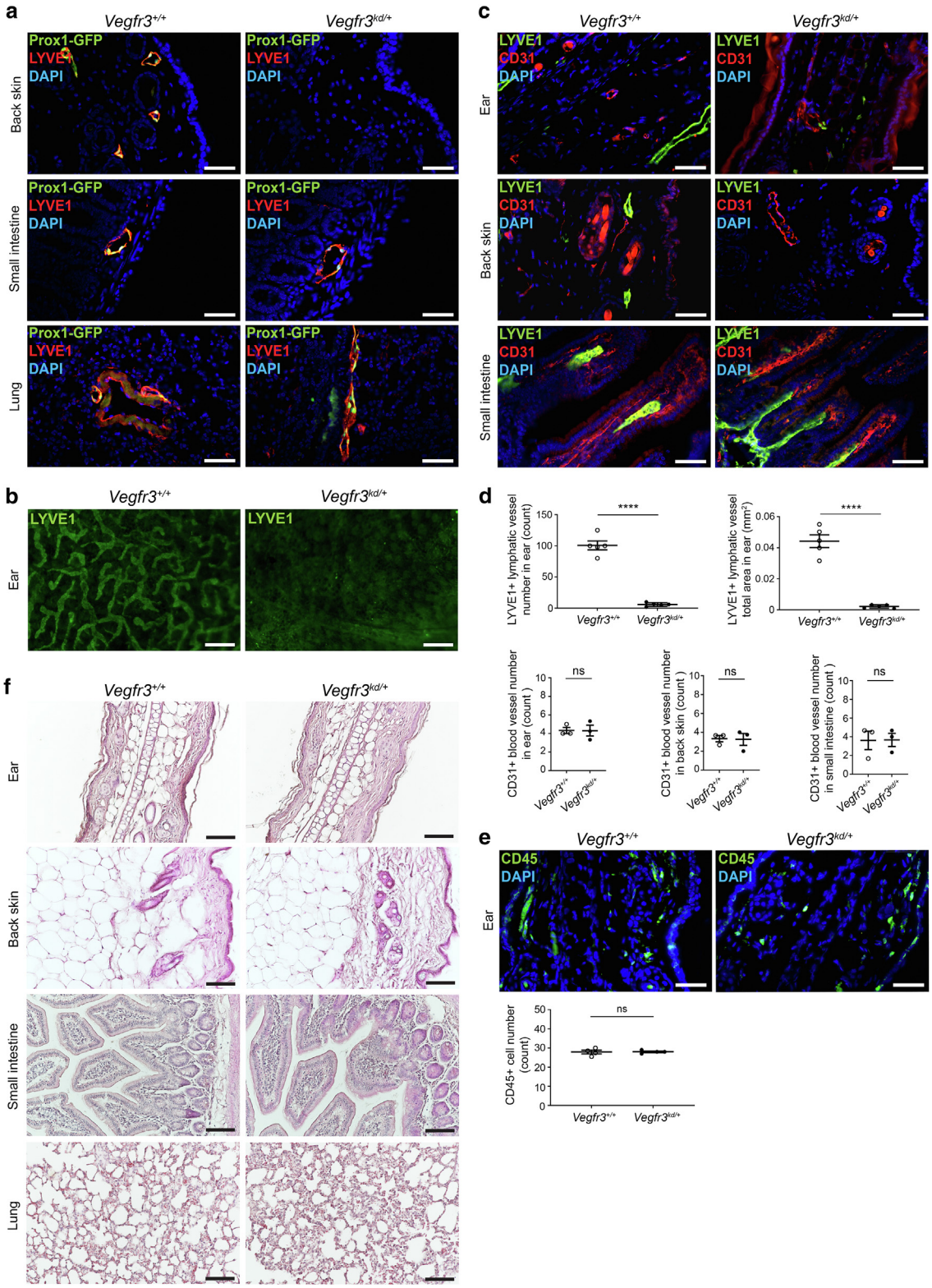

Supplementary Figure S1. Characterization of the *Vegfr3*$^{kd/+}$ mouse strain. **(a)** Anti-GFP and anti-LYVE1 fluorescent immunostaining of *Prox1*^{GFP} lymphatic reporter *Vegfr3*$^{+/+}$ and *Vegfr3*$^{kd/+}$ mice tissues. Bars =: 50 μm; n = 4 for each group. **(b)** Morphology of LYVE1^{+} structures by fluorescence stereo microscopy after whole-mount immunostaining. Bars = 500 μm; n = 3 for each group. **(c)** Anti-CD31 and anti-LYVE1 fluorescent immunohistology. Bars = 50 μm; n = 6 for *Vegfr3*$^{+/+}$ and n = 4 for *Vegfr3*$^{kd/+}$. **(d)** Quantitative data for LYVE1^{+} lymphatic vessel number and total lymphatic area in ear samples ($P = 1.1713 \times 10^{-5}$ for lymphatic vessel number and $P = 7.0627 \times 10^{-6}$ for total lymphatic vessel area; 2-tailed, unpaired *t*-test; mean ± SEM; n = 5 mice for each group) and quantitative data for CD31^{+} blood vessel number ($P = .968788$ for ear; $P = .912469$ for back skin; $P = .96516$ for small intestine; 2-tailed, unpaired *t*-test; mean ± SEM; n = 3 mice for each group). **(e)** CD45-expressing cells in ear sections by fluorescent immunostaining. Bars = 50 μm; n = 4 for each group. Quantification of CD45^{+} cells in ear sections based on fluorescent immunohistology ($P = .9072$; 2-tailed, unpaired *t*-test; mean ± SEM; n = 4 mouse ear for each group). **(f)** H&E staining on tissue sections of *Vegfr3*$^{+/+}$ and *Vegfr3*$^{kd/+}$ mice. Bars = 100 μm; n = 8 for each group. ns, not significant.

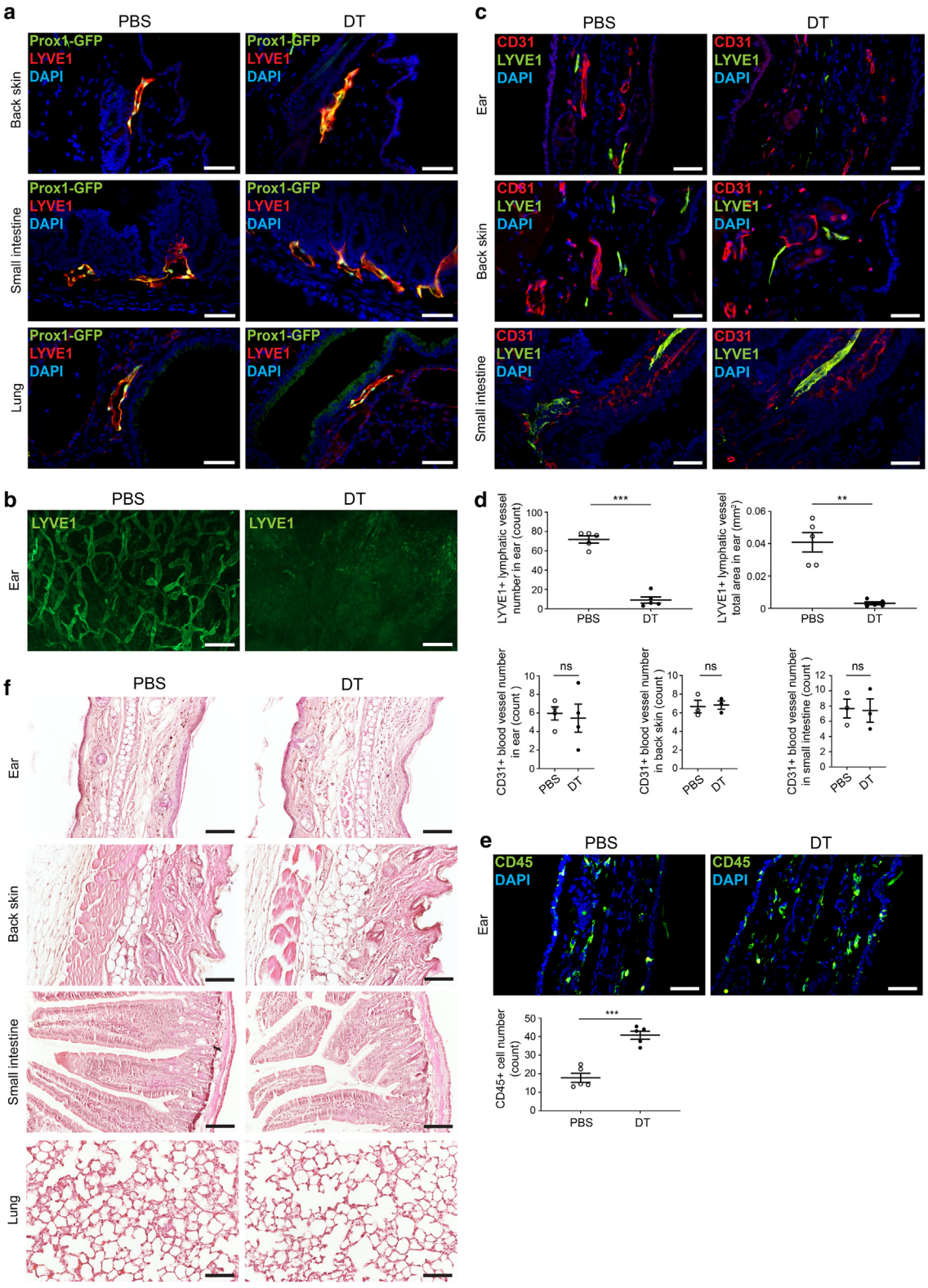

Supplementary Figure S2. Characterization of the Flt4-CreER^{T2}; *iDTR*$^{fl/+}$ mouse strain after DT injection into ear. *Prox1*^{GFP} lymphatic reporter Flt4-CreER^{T2}; *iDTR*$^{fl/+}$ mice were injected with PBS or DT into ear skin, and 8 days after the first injection, different tissue samples were collected. **(a)** Anti-GFP and anti-LYVE1 fluorescent immunostaining. Bars = 50 μm; n = 3 for each group. **(b)** Morphology of LYVE1$^+$ structures shown by fluorescence stereo microscopy after whole-mount immunostaining. Bars = 500 μm; n = 4 for each group. **(c)** Anti-CD31 and anti-LYVE1 fluorescent immunohistology. Bars = 50 μm; n = 3 for each group. **(d)** Quantitative data for LYVE1$^+$ lymphatic vessel number and total lymphatic area (P = .0002 for lymphatic vessel number and P = .0030 for total lymphatic vessel area; 2-tailed, paired t-test; mean ± SEM; n = 5 mice for each group) and quantitative data for CD31$^+$ blood vessel number (P = .70738 for ear; P = .84743 for back skin; P = .904729 for small intestine; 2-tailed, unpaired t-test; mean ± SEM; n = 3 mice for each group). **(e)** CD45-expressing cells in ear sections by fluorescent immunohistology. Bars = 50 μm; n = 5 for each group. Quantification of CD45$^+$ cells based on fluorescent immunohistology (P = .0008; 2-tailed, paired t-test; mean ± SEM; n = 5 mouse ear for each group). **(f)** H&E histology on tissue sections. Bars = 100 μm; n = 3 for each group. DT, diphtheria toxin.

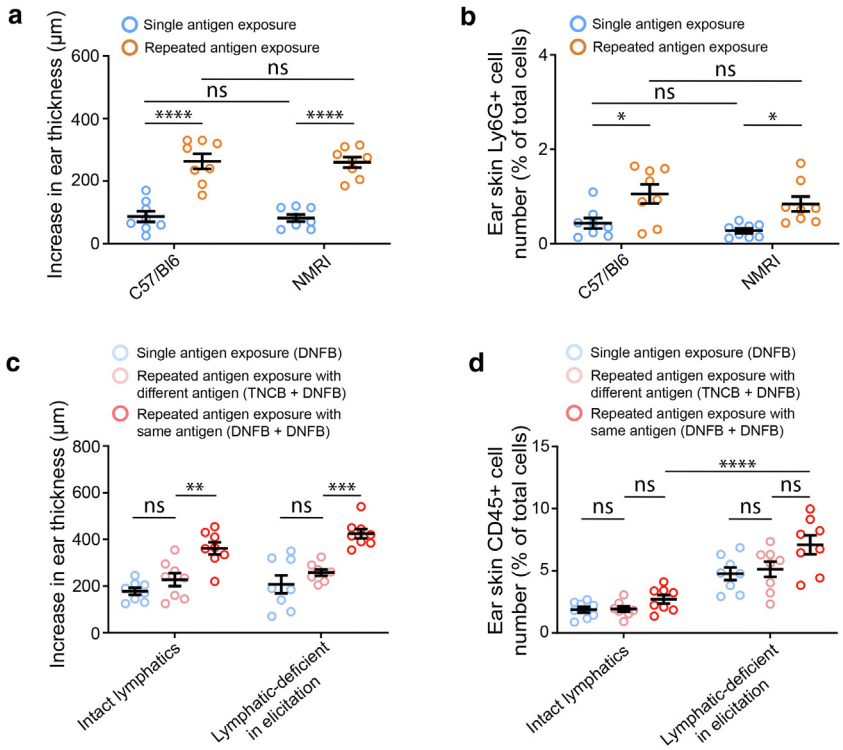

Supplementary Figure S3. Antigen specificity of contact hypersensitivity response. **(a)** The increase in ear thickness of mice with intact lymphatics from C57/Bl6 and NMRI genetic background (2-way ANOVA with Tukey's multiple comparisons test; mean ± SEM; n = 8 for each group; $P < .0001$ for C57/Bl6 after single vs repeated antigen exposure; $P < .0001$ for NMRI after single vs repeated antigen exposure; $P = .9972$ for C57/Bl6 vs NMRI after single antigen exposure; $P = .9993$ for C57/Bl6 vs NMRI after repeated antigen exposure). **(b)** $Ly6G^+$ immune cell numbers represented in ears with intact lymphatics of C57/Bl6 and NMRI mice measured by CytoFLEX (2-way ANOVA with Tukey's multiple comparisons test; mean ± SEM; n = 8 for each group; $P = .0218$ for C57/Bl6 after single vs repeated antigen exposure; $P = .0407$ for NMRI after single vs repeated antigen exposure; $P = .8566$ C57/Bl6 vs NMRI after single antigen exposure; $P = .7136$ for C57/Bl6 vs NMRI mice after repeated antigen exposure). **(c)** The increase in ear thickness of mice with intact lymphatics or lymphatic deficiency after single (DNFB), repeated exposure with a different (TNCB and DNFB), or the same antigen (DNFB and DNFB) (2-way ANOVA with Tukey's multiple comparisons test; mean ± SEM; n = 8 for each group; $P = .7186$ for intact lymphatics after single vs repeated with different antigen; $P = .7081$ for lymphatic deficiency after single vs repeated with different antigen; $P = .0058$ for intact lymphatics after repeated with different vs same antigen; $P = .0004$ for lymphatic deficiency after repeated with different vs same antigen). **(d)** $CD45^+$ immune cell numbers are represented in ears of mice with intact lymphatics or lymphatic deficiency measured by CytoFLEX (2-way ANOVA with Tukey's multiple comparisons test; mean ± SEM; n = 8 for each group; $P > .9999$ for intact lymphatics after single vs repeated with different antigen; $P = .9947$ for lymphatic deficiency after single vs repeated with different antigen; $P = .8629$ for intact lymphatics after repeated with different vs same antigen; $P = .0703$ for lymphatic deficiency after repeated with different vs same antigen; $P < .0001$ for intact vs lymphatic deficiency after repeated with same antigen). DNFB, 2,4-dinitro-1-fluorobenzene; ns, not significant; TNCB, 2-chloro-1,3,5-trinitrobenzene.

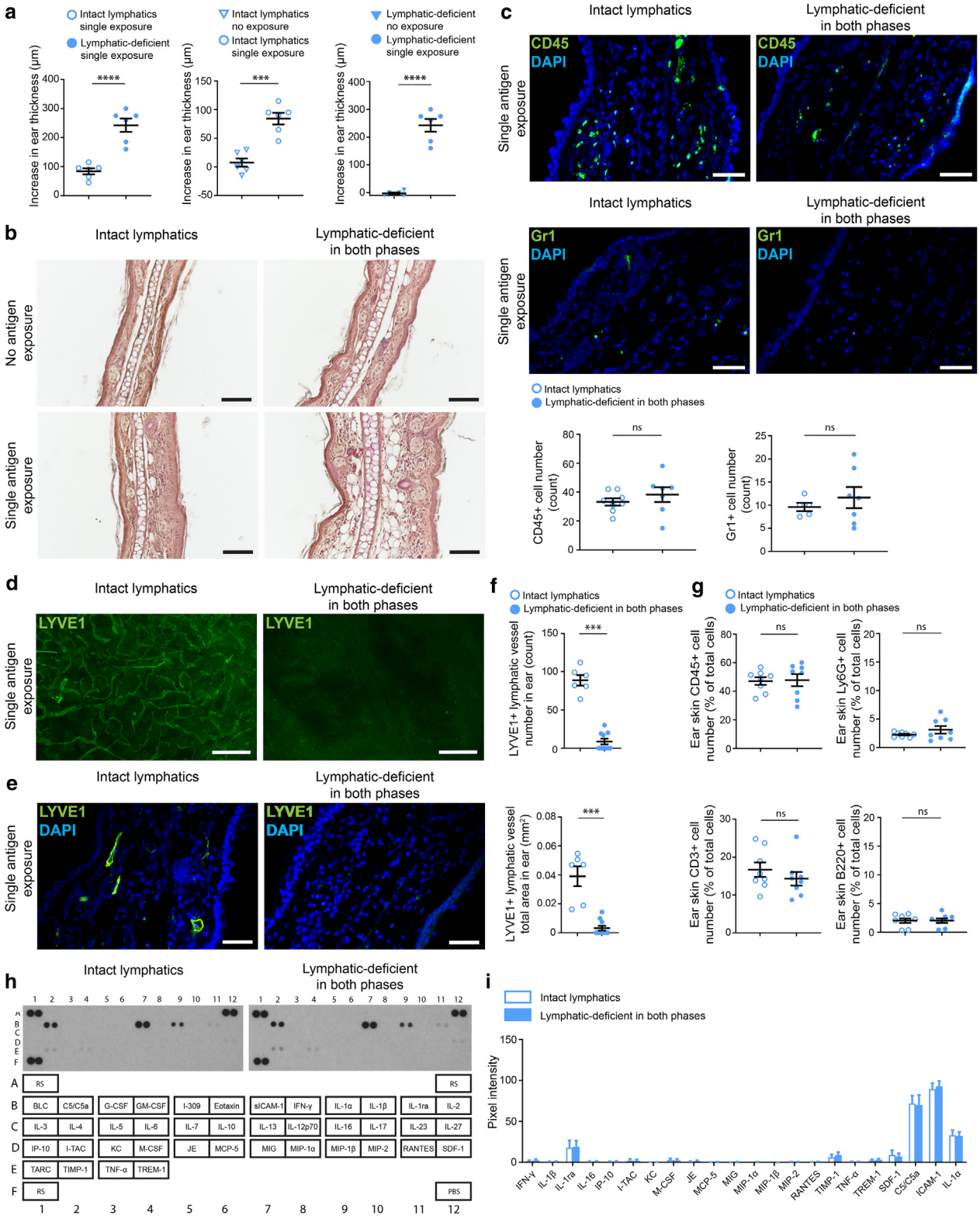

Supplementary Figure S4. Effect of single antigen exposure in mice lacking lymphatics in the sensitization and elicitation phase of CHS. Mice with normal lymphatics or dermal lymphatic deficiency in both phases were treated with acetone vehicle on the abdominal skin, and 5 days after exposure, acetone vehicle or single antigen treatment was performed on ear skin. **(a)** The increase in ear thickness ($P < .0001$ for mice with normal lymphatics vs dermal lymphatic-deficient mice after single exposure, $P = .0001$ for mice with intact lymphatics with no exposure vs single exposure, $P = 9.5617 \times 10^{-7}$ for mice with dermal lymphatic deficiency with no exposure vs single exposure; 2-tailed, unpaired *t*-test, mean ± SEM; n = 6 mouse ear for each group). **(b)** H&E histology on ear skin sections. Bars = 100 μm; n = 4 for each group. **(c)** CD45- and GR1-expressing immune cells visualized in ear sections by fluorescent immunostaining. Bars = 50 μm; n = 5 for each group. Quantification of immune cells in ear sections based on fluorescent immunohistology ($P = .3754$ for $CD45^+$ cells and $P = .4864$ for $GR1^+$ cells; 2-tailed, unpaired *t*-test; mean ± SEM; n = 5 mouse ear for each group). **(d)** LYVE1-expressing structures shown by stereo microscopy after whole-mount immunostaining. Bars = 500 μm; n = 3 for each group. **(e)** Anti-LYVE1 fluorescent immunohistology of ear sections. Bars = 50 μm; n = 8 and n =

12 for the groups with intact lymphatics and lymphatic-deficient in both phases, respectively. **(f)** Number of lymphatic vessels and total lymphatic area in ear sections ($P = .0002$ for lymphatic vessel number and $P = .0001$ for total lymphatic area; Mann–Whitney *U* test; mean ± SEM; n = 6 for and n = 10 for the groups with intact lymphatics and lymphatic deficiency, respectively). **(g)** Quantitative flow cytometry data for immune cell numbers in mouse ears ($P = .8955$ for $CD45^+$ cells, $P = .2370$ for $Ly6G^+$ cells, $P = .3779$ for $CD3^+$ cells, and $P = .9865$ for $B220^+$ cells; 2-tailed, unpaired *t*-test; mean ± SEM; n = 8 mouse ear for each group). **(h)** Cytokine array to detect cytokine expression in ear tissue supernatants. Representative images showing the position of the cytokines in duplicates (n = 3 for each group). Data shown are from a 5-minute exposure to the X-ray film. **(i)** Summary graph of the quantification of the cytokine array representing the pixel density of images of mouse ears (2-tailed, unpaired *t*-test; mean ± SEM; n = 3 mouse ear for each group). CHS, contact hypersensitivity; ns, not significant; RS, reference spot.

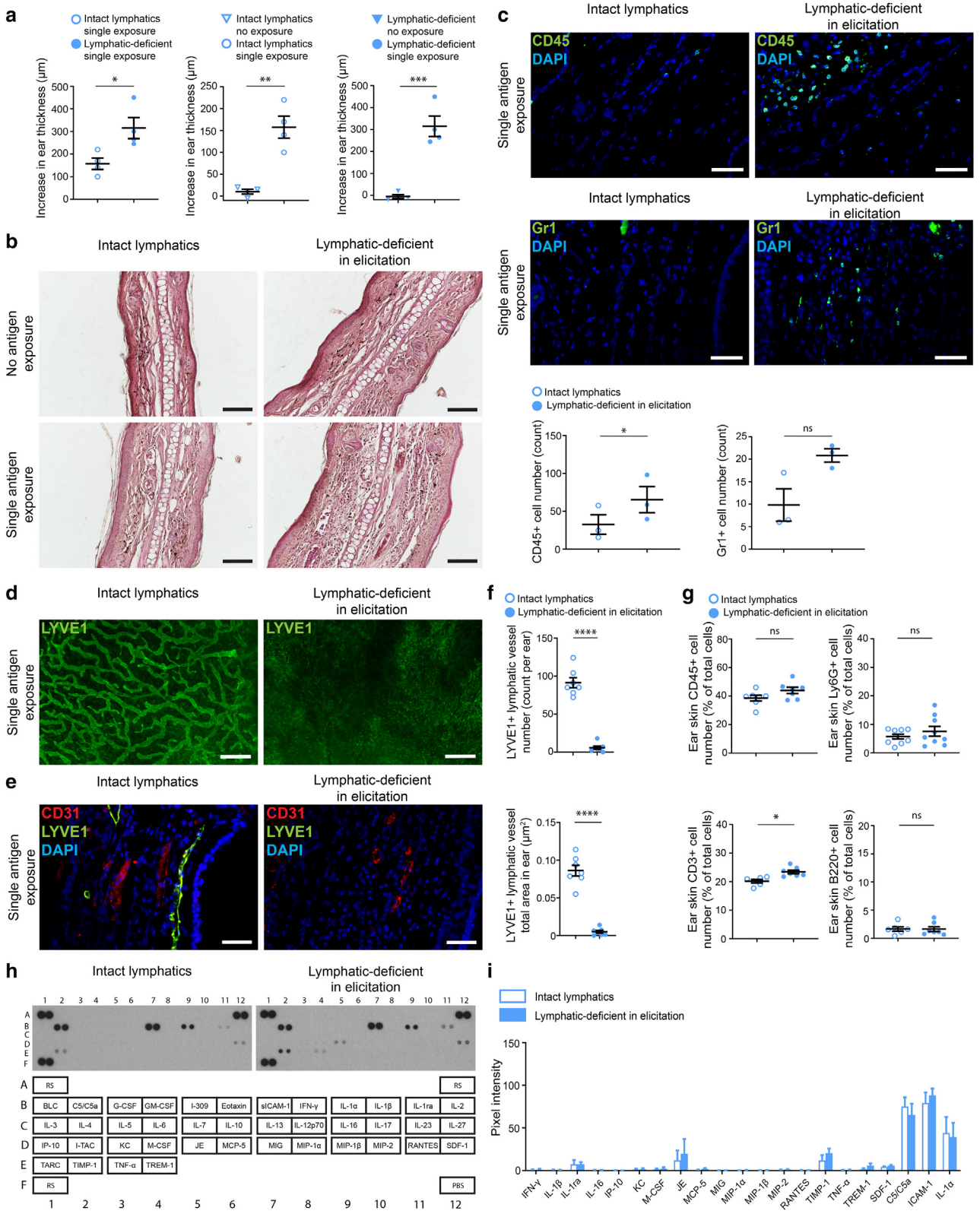

Supplementary Figure S5. Effect of single antigen exposure in mice lacking lymphatics in the elicitation phase of CHS. Mice with normal lymphatics or local lymphatic deficiency in the elicitation phase were treated with acetone vehicle on the abdominal skin, and 5 days after exposure, acetone vehicle or single antigen treatment was performed on ear skin. **(a)** The increase in ear thickness ($P = .0187$ for mice with normal lymphatics vs lymphatic deficiency after single exposure, 2-tailed, paired *t*-test; $P = .0013$ for mice with intact lymphatics with no exposure vs single exposure, $P = 0.0005$ for mice with lymphatic deficiency with no exposure vs single exposure; 2-tailed, unpaired *t*-test, mean ± SEM; n = 4 mouse ear for each group). **(b)** H&E histology of ear skin sections. Bars = 100 μm; n = 4 for each group. **(c)** CD45- and GR1-expressing immune cells in ear sections by fluorescent immunohistology. Bars = 50 μm; n = 3 for each group. Quantification of immune cells in ear sections of mice with intact lymphatics or lymphatic-deficient mice in elicitation was calculated on the basis of fluorescent immunohistology ($P = .0207$ for $CD45^+$, $P = .1592$ for $GR1^+$ cells; 2-tailed, paired *t*-test; mean ± SEM; n = 3 for each group). **(d)** LYVE1-expressing

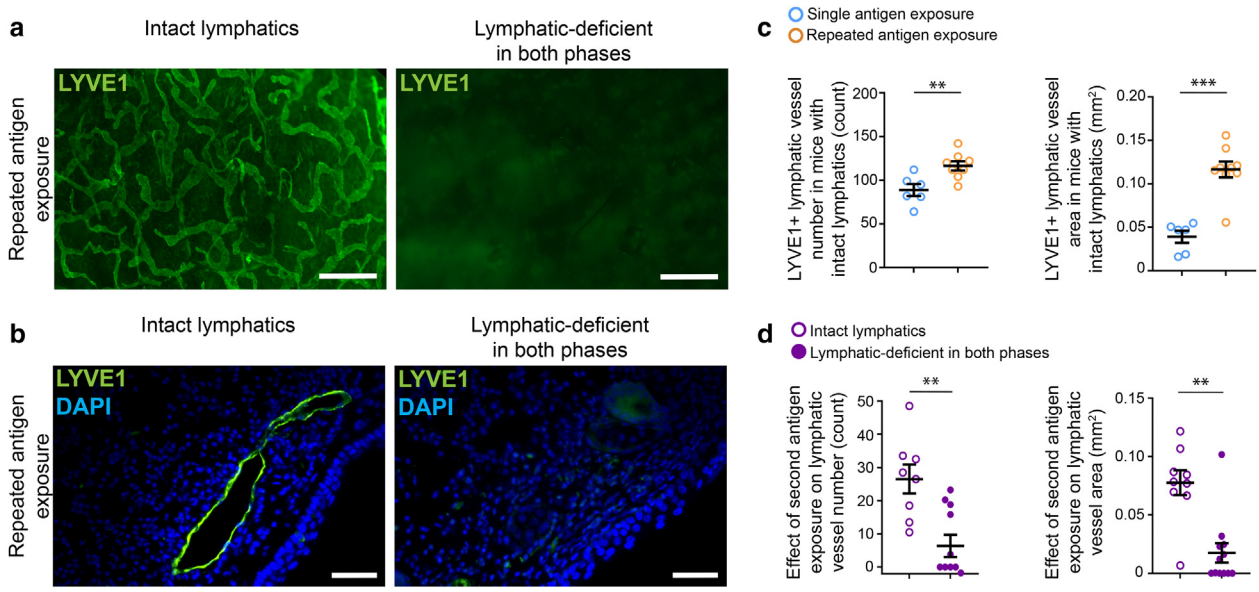

Supplementary Figure S6. Lymphatic morphology shown in mouse ear lacking lymphatic vessels in both phases after repeated antigen treatment. Mice with normal lymphatics or dermal lymphatic deficiency were treated with antigen on the abdominal skin, and 5 days after exposure, antigen treatment was repeated on the ear skin. **(a)** LYVE1-expressing structures detected by stereo microscopy after whole-mount immunostaining of ear samples. Bars = 500 μm; n = 3 for each group. **(b)** Anti-LYVE1 fluorescent immunohistology of ear sections. Bars = 50 μm; n = 12 for each group. **(c)** Number of lymphatic vessels and total lymphatic area in ear sections after single or repeated antigen exposure ($P = .0068$ for lymphatic vessel number; 2-tailed, unpaired *t*-test; mean ± SEM; n = 6 for and n = 8 for the groups with single and repeated antigen exposure, respectively; $P = .0004$ for total lymphatic area; Mann–Whitney *U* test; mean ± SEM; n = 6 and n = 9 for the groups with single and repeated antigen exposure). **(d)** The effects of the second antigen exposure to the lymphatic vessel number and area are calculated by subtracting the mean of corresponding control group values after single exposure ($P = .0017$ for lymphatic vessel number; 2-tailed, unpaired *t*-test; mean ± SEM; n = 8 and n = 11 for the groups with intact lymphatics and lymphatic deficiency in both phases; $P = .0017$ for total lymphatic area; Mann–Whitney *U* test; mean ± SEM; n = 8 and n = 11 for the groups with intact lymphatics and lymphatic deficiency, respectively).

structures detected by stereo microscopy after whole-mount immunostaining of ear samples. Bars = 500 μm; n = 6 for each group. **(e)** Anti-CD31 and anti-LYVE1 fluorescent immunohistology of ear sections. Bars = 50 μm; n = 3 for each group. **(f)** Number of lymphatic vessels and total lymphatic area in ear sections ($P = 2.1607 \times 10^{-6}$ for lymphatic vessel number and $P = 7.1126 \times 10^{-5}$ for total lymphatic area; 2-tailed, paired *t*-test; mean ± SEM; n = 7 for each group). **(g)** Quantitative flow cytometry data for immune cell numbers represented in ears ($P = .0834$ for $CD45^+$ cells, $P = .1853$ for $Ly6G^+$ cells, and $P = .0144$ for $CD3^+$ cells, 2-tailed, paired *t*-test; $P = .8438$ for $B220^+$ cells, Wilcoxon signed-rank test; mean ± SEM; n = 9 and n = 10 for the groups with intact lymphatics and lymphatic deficiency, respectively). **(h)** Cytokine array to detect cytokine expression in ear tissue supernatants. Representative images showing the position of the cytokines in duplicates (n = 3 for each group). Data shown are from a 10-minute exposure to the X-ray film. **(i)** Summary graph of the quantification of the cytokine array representing the pixel density of X-ray film in ears (2-tailed, paired *t*-test; mean ± SEM; n = 3 mouse ear for each group).

CHS, contact hypersensitivity; ns, not significant; RS, reference spot.

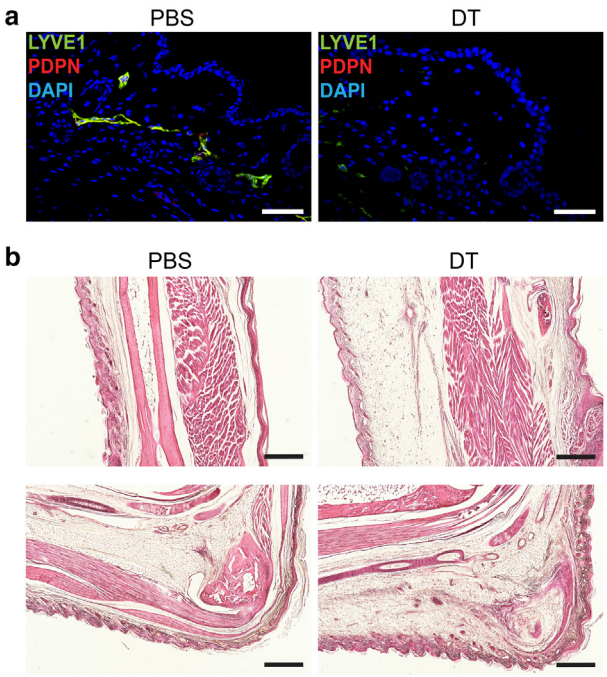

Supplementary Figure S7. Local deletion of lymphatic vessels in the hind paw of Flt4-CreER^{T2}; *iDTR*$^{fl/fl}$ mice by DT injection. **(a)** LYVE1- and PDPN-expressing structures shown in hind paw. Bars = 50 μm; n = 8 for each group. **(b)** H&E staining of hind paw sections of mice with intact lymphatics or lymphatic deficiency only in sensitization 8 days after injection with PBS or DT. Bars = 500 μm; n = 6 for each group. DT, diphtheria toxin.

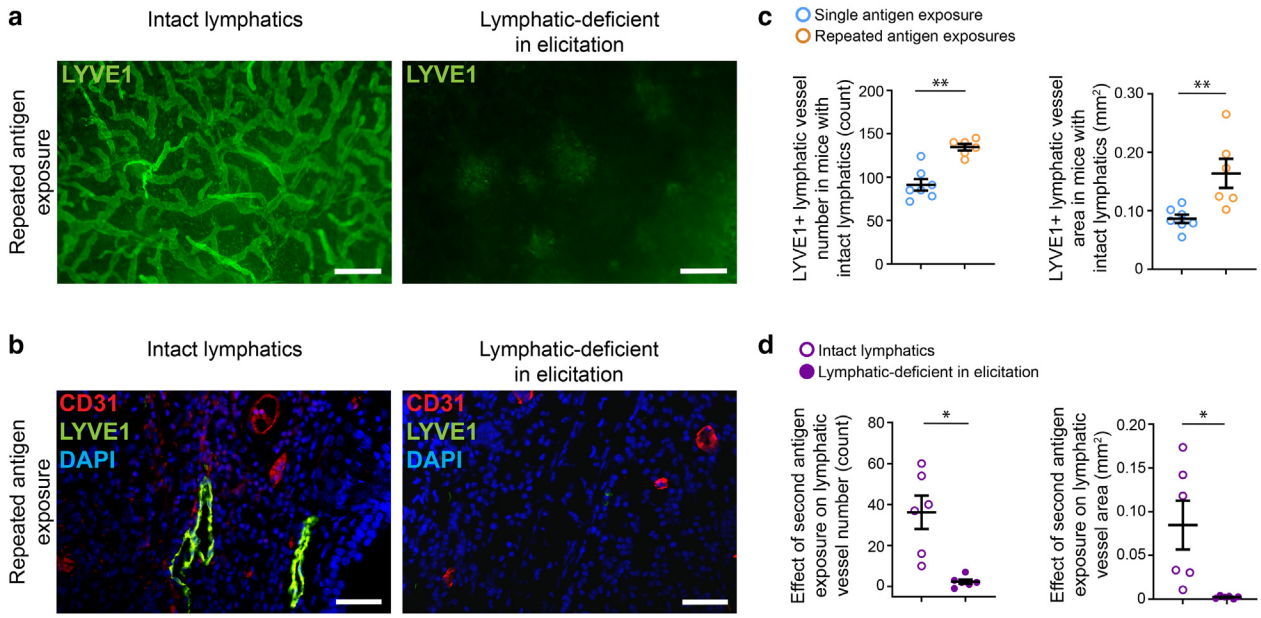

Supplementary Figure S8. Lymphatic morphology shown in mouse ears lacking lymphatic vessels only in the elicitation phase after repeated antigen treatment. Mice with normal lymphatics or local lymphatic deficiency in the ear were treated with antigen on the abdominal skin, and 5 days after exposure, antigen treatment was repeated on the ear skin. **(a)** LYVE1-expressing structures detected by stereo microscopy after whole-mount immunostaining of ear samples. Bars = 500 μm; n = 6 for each group. **(b)** Anti-CD31 and anti-LYVE1 fluorescent immunohistology of ear sections. Bars = 50 μm; n = 3 for each group. **(c)** Number of lymphatic vessels and total lymphatic area in ear sections ($P = .0002$ for lymphatic vessel number; $P = .0082$ for total lymphatic area; 2-tailed, unpaired *t*-test; mean ± SEM; n = 7 and n = 6 for the groups with single and repeated exposure). **(d)** The effect of the second antigen exposure is calculated by subtracting the mean of the corresponding control group values after single antigen exposure ($P = .0116$ for lymphatic vessel number and $P = .0322$ for total lymphatic area; 2-tailed, paired *t*-test; mean ± SEM; n = 6 for each group).